Science of the Total Environment 812 (2022) 152474

Contents lists available at ScienceDirect

Science of the Total Environment

journal homepage: www.elsevier.com/locate/scitotenv

Influence of environmental variability and *Emiliania huxleyi* ecotypes on alkenone-derived temperature reconstructions in the subantarctic Southern Ocean

A.S. Rigual-Hernández [a,*], F.J. Sierro [a], J.A. Flores [a], T.W. Trull [b,c,d], T. Rodrigues [e,f], B. Martrat [g], E.L. Sikes [h], S.D. Nodder [i], R.S. Eriksen [b,c], D. Davies [b,d], N. Bravo [g], J.M. Sánchez-Santos [j], F. Abrantes [e,f]

[a] *Área de Paleontología, Departamento de Geología, Universidad de Salamanca, 37008 Salamanca, Spain*
[b] *CSIRO Oceans and Atmosphere, Hobart, Tasmania 7001, Australia*
[c] *Institute for Marine and Antarctic Studies, University of Tasmania, Private Bag 129, Hobart, Tasmania 7001, Australia*
[d] *Antarctic Climate and Ecosystems Cooperative Research Centre and Australian Antarctic Program Partnership, University of Tasmania, Hobart, Tasmania 7001, Australia*
[e] *Portuguese Institute for Sea and Atmosphere (IPMA), Divisão de Geologia Marinha (DivGM), Rua Alfredo Magalhães Ramalho 6, Lisboa, Portugal*
[f] *CCMAR, Centro de Ciências do Mar, Universidade do Algarve, Campus de Gambelas, 8005-139 Faro, Portugal*
[g] *Department of Environmental Chemistry, IDAEA-CSIC, 08034 Barcelona, Spain*
[h] *Marine and Coastal Sciences, Rutgers University, New Brunswick, NJ, USA*
[i] *National Institute of Water and Atmospheric Research, Wellington 6021, New Zealand*
[j] *Departamento de Estadística, Universidad de Salamanca, 37008 Salamanca, Spain*

HIGHLIGHTS

- Alkenone fluxes were monitored during a year in the Subantarctic Zone.
- Temperature reconstructions mirrored SSTs except for late winter.
- Alkenone-derived SSTs increased with depth in the water column.
- Deviations of alkenone-derived SSTs were correlated with *E. huxleyi* ecotypes.
- *Emiliania huxleyi* diversity may bias SST reconstructions in the Southern Ocean.

GRAPHICAL ABSTRACT

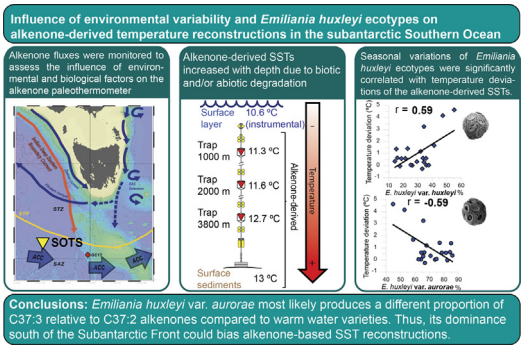

ARTICLE INFO

Article history:
Received 12 July 2021
Received in revised form 10 December 2021
Accepted 13 December 2021
Available online 22 December 2021

Editor: Ashantha Goonetilleke

ABSTRACT

Long-chain unsaturated alkenones produced by haptophyte algae are widely used as paleotemperature indicators. The unsaturation relationship to temperature is linear at mid-latitudes, however, non-linear responses detected in subpolar regions of both hemispheres have suggested complicating factors in these environments. To assess the influence of biotic and abiotic factors in alkenone production and preservation in the Subantarctic Zone, alkenone fluxes were quantified in three vertically-moored sediment traps deployed at the SOTS observatory (140°E, 47°S) during a year. Alkenone fluxes were compared with coccolithophore assemblages, satellite measurements and surface-water properties obtained by sensors at SOTS. Alkenone-based temperature reconstructions generally mirrored the seasonal variations of SSTs, except for late winter when significant deviations were observed (3–10 °C). Annual flux-weighted averages in the 3800 m trap returned alkenone-derived temperatures ~1.5 °C warmer than those derived from the 1000 m trap, a distortion attributed to surface production and signal preservation during its transit through the water column. Notably, changes in the relative abundance of *E. huxleyi* var. *huxleyi* were positively correlated with

* Corresponding author.
E-mail address: arigual@usal.es (A.S. Rigual-Hernández).

http://dx.doi.org/10.1016/j.scitotenv.2021.152474

temperature deviations between the alkenone-derived temperatures and in situ SSTs (r = 0.6 and 0.7 at 1000 and 2000 m, respectively), while *E. huxleyi* var. *aurorae*, displayed an opposite trend. Our results suggest that *E. huxleyi* var. *aurorae* produces a higher proportion of $C_{37:3}$ relative to $C_{37:2}$ compared to its counterparts. Therefore, the dominance of var. *aurorae* south of the Subtropical Front could be at least partially responsible for the less accurate alkenone-based SST reconstructions in the Southern Ocean using global calibrations. However, the observed correlations were largely influenced by the samples collected during winter, a period characterized by low particle fluxes and slow sinking rates. Thus, it is likely that other factors such as selective degradation of the most unsaturated alkenones could also account for the deviations of the alkenone paleothermometer.

1. Introduction

1.1. Background and objectives

Under the influence of global climate change, the polar oceans are continuing to warm, with the Southern Ocean south of 30°S accounting for ca. 40% of the global ocean heat gain in the upper 2000 m (Pörtner et al., 2019). In order to be able to put the magnitude and rate of the ongoing and projected climate change into a longer-term context, it is essential to compare modern instrumental temperature data with pre-instrumental temperature variations. Alkenones are a class of unsaturated long-chain methyl and ethyl ketones with a variable degree of unsaturation that represent one of the most robust proxies for the reconstruction of past sea-surface temperatures (SSTs) (Brassell et al., 1986; Conte et al., 2006; Martrat et al., 2007; Liu et al., 2009; Sikes et al., 2009; Sikes et al., 2019; Wang et al., 2021). They are linear methyl and ethyl C31: to C43: ketones with 2, 3 or 4 double bounds and trans configuration (Boon and de Leeuw, 1979; López and Grimalt, 2004). Their production is taxonomically restricted to certain Prymnesiophyte algae of the order Isochrydales, primarily to the genera *Isochrysis*, *Chrysotila*, *Emiliania* and *Gephyrocapsa* (Volkman et al., 1980; Sukenik and Wahnon, 1991; Volkman et al., 1995; Eltgroth et al., 2005; Jaraula et al., 2010; Wang et al., 2021). In the modern pelagic ocean, the production of alkenones is mainly limited to the coccolithophores *Emiliania huxleyi* and *Gephyrocapsa oceanica*, but other species may also play a role (Conte et al., 1995; Volkman et al., 1995; Wang et al., 2021).

The proportion of di- to tri- unsaturated C_{37} methyl alkenones, expressed as $U^{K'}_{37} = C_{37:2} / (C_{37:2} + C_{37:3})$, is linearly correlated with water temperatures in cell cultures, sediment trap records and the global ocean marine sediments, between 60°N and 60°S (Brassell et al., 1986; Prahl and Wakeham, 1987; Prahl et al., 1988; Müller et al., 1998; Conte et al., 2006). Using a global compilation of surface sediment samples, Müller et al. (1998) developed one of the first global calibrations of $U^{K'}_{37}$ ($U^{K'}_{37} = 0.033\,T + 0.044$, $r^2 = 0.958$), that provided further evidence of the robustness of alkenone paleothermometry. However, despite the overall good correlation between alkenone-derived SSTs and modern SSTs, weaker responses at low (e.g. Sonzogni et al., 1997; Herbert, 2001) and high latitude systems have been documented (e.g. Sikes and Volkman, 1993; Sikes et al., 1997; Rosell-Melé et al., 2000; Sikes et al., 2009; Prahl et al., 2010; Max et al., 2020). The U^{K}_{37} index that also incorporates the tetra-unsaturated compound, has been used to improve SST reconstructions in the North Atlantic suggesting this index might be more useful at high latitudes (Bard et al., 2000; Bendle and Rosell-Melé, 2004). However, in the Southern Ocean, this index has not been shown to be better correlated to SST (Sikes et al., 1997; Ho et al., 2012) (Sikes et al., 1997, Ho 2021).

In the Southern Ocean south of Tasmania Sikes et al. (2009) identified that accuracy of the reconstruction of Late Holocene sea-surface temperatures (SSTs) based on $U^{K'}_{37}$ from several sediment cores retrieved from locations north and south of the Subtropical Front depended on the calibration chosen. Reconstructions made with the calibration of Prahl et al. (1988) ($U^{K'}_{37} = 0.034\,T + 0.039$) provided accurate values for the sediment core-tops but reconstructions for the subantarctic sediments were about 2 °C too cool. In turn, the most accurate reconstructions in subantarctic waters were obtained when applying the regional calibration for the Southern Ocean developed by Sikes and Volkman (1993) ($U^{K'}_{37} = 0.00414T–0.156$). Non-thermal factors, such as light and nutrient stress (Prahl et al., 2003), selective degradation of C_{37} alkenones (Rontani et al., 2013), lateral advection (Rosell-Melé et al., 2000), seasonal variations in the alkenone production (e.g. Sikes et al., 1997; Sikes et al., 2005; Harada et al., 2006; Max et al., 2020), and inter- and intraspecific variability of the alkenone-synthesizing algal populations (Volkman et al., 1995; Sawada et al., 1996; Conte et al., 1998; Popp et al., 1998) have all been invoked as possible sources of variability in the $U^{K'}_{37}$ imprint preserved in the sedimentary record. The lack of understanding on how these factors influence the biosynthesis and subsequent preservation of alkenones in the sedimentary record limits the accuracy of the paleotemperature reconstructions in the subantarctic Southern Ocean.

In order to shed light on these issues, we examine the alkenone fluxes collected by three vertically-moored sediment traps deployed during a year (August 2011 to July 2012) at the Southern Ocean Time Series (SOTS) observatory in the Subantarctic Zone (SAZ), southwest of Tasmania, Australia (Trull et al., 2010; Eriksen et al., 2018). These flux measurements are compared with the coccolithophore fluxes and in situ environmental measurements during the same time interval (Rigual-Hernández et al., 2020b; Rigual-Hernández et al., 2020c) and with alkenone-derived paleotemperature records from a nearby deep-sea sediment core (Sikes et al., 2009). The combination of biomarker and taxonomic analyses with environmental monitoring conducted at SOTS allows us to provide new insights into the role of biotic and abiotic factors in the controls of alkenone unsaturation, with implications for alkenone-based oceanographic reconstructions.

1.2. Oceanographic setting

The Southern Ocean is subdivided by a series of oceanographic fronts that delimit different zonal systems (Fig. 1) of relatively uniform physical, chemical and biological properties (Orsi et al., 1995; Rintoul and Trull, 2001; Trull et al., 2001b). In the Australian-Tasmanian region, the Australian mainland demarcates the northern boundary of the subtropical gyres. Then from north to south, the fronts and zones are defined as follows: the Subtropical Front (STF; at ~46°S; Fig. 1), the SAZ, the Subantarctic Front (SAF; at ~51°S), Polar Frontal Zone (PFZ), Polar Front (PF), and the Antarctic Zone (AZ). The STF is characterized by a marked temperature gradient of 4 °C in less than 0.5° of latitude between the subtropical and subantarctic waters (Deacon, 1982; Belkin and Gordon, 1996; Rintoul et al., 1997). This temperature gradient persists despite the annual seasonal cycle in SSTs. South of Tasmania, summer SSTs are about 16° and 12 °C in subtropical and subantarctic waters, respectively. During winter, SSTs are about 12° and 8 °C, respectively, in these surface water masses (Belkin and Gordon, 1996; Rintoul et al., 1997). In the central parts of the ocean basins, away from shallow bathymetry, the meridional position of the STF is primarily controlled by winds and displays substantial seasonal to decadal variability in those regions where it is not constrained bathymetrically (Behrens et al., 2021 and references therein). In the waters south of Tasmania, the position of the STF is dominated by mesoscales processes. The STF moves southward during summertime, while during winter is located further north. Fig. 1 shows the range of the seasonal variability of the STF (based on the Orsi et al. (1995) definition, i.e. 11 degree isotherm at 100 m) for the period 2004–2018 and for the sediment trap deployment period (i.e. August 2011 to August 2012). During the field experiment the STF

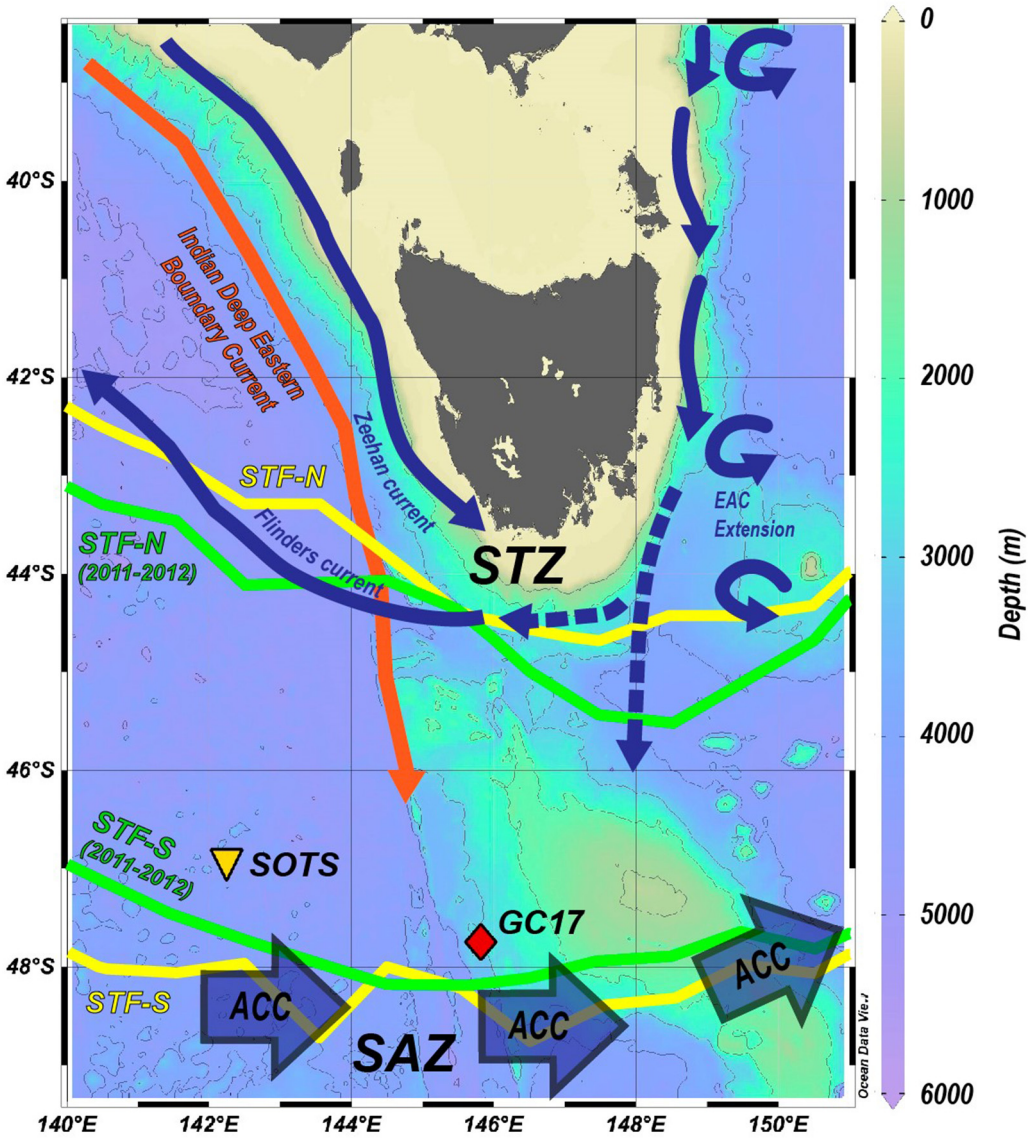

Fig. 1. Bathymetric map of the study region south of Tasmania showing the location of Southern Ocean Time Series (SOTS) observatory (yellow triangle) and core GC17 (grey diamond). Blue arrows indicate the approximate surface circulation (after Pardo et al., 2019) and the grey arrow shows the Indian Deep Eastern Boundary current circulation (1500 and 3000 m; Tamsitt et al., 2019). The two dotted currents indicate the seasonal water transport (mostly during austral summer) from the EAC extension towards the west of Tasmania and the Southern Ocean (van Sebille et al., 2012). The maximum north and south locations of the STF based on the Orsi definition (11 degree isotherm at 100 m) for the period 2004–2018 (climatology) and for the study interval (August 2011–August 2012) are represented as yellow and green lines, respectively. The underlying temperature data is from Roemmich-Gilson Argo climatology (Roemmich and Gilson, 2009).Abbreviations: STZ – Subtropical Zone, STF – Subtropical Front (after Orsi et al. (1995)), SAZ – Subantarctic Zone. EAC – East Australian Current, and ACC – Antarctic Circumpolar Current. Bathymetric data from General Bathymetric Chart of the Oceans (2020) (doi:10.5285/a29c5465-b138-234d-e053-6c86abc040b9). Ocean Data View software (Schlitzer, 2021) was used to generate this figure.

was located north of SOTS observatory except for a three-month interval during summer-autumn (March to May 2012). Additionally, it is important to note that at meso-bathypelagic depths (~1500–3000 m depth) southwest of Tasmania a branch of the deep eastern Indian Ocean boundary current flows into the Antarctic Circumpolar Current (ACC) (Tamsitt et al., 2019), and therefore it may potentially reach the location of the SOTS observatory (see Section 3 for further details). At the surface in the Subtropics, the Zeehan Current (an extension of the Leeuwin Current) flows southwards along the west coast of Tasmania (Ridgway, 2007). East of Tasmania, a southward extension of the East Australian Current transports warm subtropical water poleward. The portion of the East Australian Current extension that reaches south of Tasmania, primarily forms the Flinders Current that flows northwest while some water is directed towards the southeast in the form of eddies (van Sebille et al., 2012; Pardo et al., 2019). South of the STF, the circulation in the Subantarctic Zone is dominated by the ACC (Fig. 1) that is driven by westerly wind stress blowing over the Southern Ocean. The outcropping of deep-water masses in the SAZ generates different physical and chemical properties in the surface waters on either side of the subtropical front. Subantarctic surface waters are rich in macronutrients and cold while the subtropical gyres exhibit nutrient-depleted and warmer waters (Trull et al., 2001b). Consequently, the Subtropical and Subantarctic Zones host substantially different phytoplankton communities (Odate and Fukuchi, 1995; Kopczynska et al., 2001; Eriksen et al., 2018).

1.3. Distribution of Emiliania huxleyi morphotypes in the waters south of Tasmania

Coccolithophore assemblages in the waters south of Tasmania are dominated by *E. huxleyi* (Findlay and Giraudeau, 2000; Cubillos et al., 2007; Rigual-Hernández et al., 2020c), which is primarily composed of three

morphotypes: A overcalcified (A o/c), A and B/C (Cubillos et al., 2007; Cook et al., 2011; Cook et al., 2013). Each of these morphotypes are characterized by a particular coccolith shape, structure and degree of calcification, photosynthetic pigment composition and differing responses to environmental change (Cook et al., 2011; Cook et al., 2013; Krueger-Hadfield et al., 2014; Müller et al., 2015) that is reflected in their different latitudinal (Cubillos et al., 2007; Poulton et al., 2013; Patil et al., 2014; Malinverno et al., 2015) and seasonal distributions (Rigual-Hernández et al., 2020b). In the waters south of Tasmania, type A o/c exhibits peak abundances in the Subtropical Zone, morphotype A is most abundant between 43° and 53°S and morphotype B/C dominates coccolithophore populations in the Subantarctic Zone and becomes the only morphotype present in the Antarctic Zone (Cubillos et al., 2007; Rigual Hernández et al., 2018). Additionally, morphotypes B and C have also been documented in the Subantarctic Southern Ocean (Patil et al., 2014; Saavedra-Pellitero et al., 2014; Rigual-Hernández et al., 2020b). The differentiation of these morphotypes from type B/C is mainly based in size and it is not always possible to discriminate between them (Young et al., 2003; Cubillos et al., 2007). Cook et al. (2013) conducted a population genetic analysis on 273 *E. huxleyi* clonal cultures retrieved from the main current systems south of Australia and Southern Ocean and only two genetic varieties or ecotypes were recognized: *E. huxleyi* var. *huxleyi* and *E. huxleyi* var. *aurorae*. Based on the above mentioned studies, we refer to type A and type A o/c as *E. huxleyi* var. *huxleyi* while all members of morphogroup B, i.e. B/C, C and B (Young et al., 2021) found in the subantarctic waters south of Tasmania, are referred to as ecotype *E. huxleyi* var. *aurorae*. The ecotype *aurorae* is a Southern Ocean specialist adapted to grow under low-light regimes and at cold temperatures (Cook et al., 2011) and substantially more sensitive to ocean acidification than its counterparts (Müller et al., 2015). It is important to note that *E. huxleyi* morphotypes have been observed to display pronounced seasonal variations in their relative abundance at SOTS. Moreover, the coccoliths collected by the traps have been reported to display an excellent preservation thereby indicating that negligible calcite dissolution occurs in their transit throughout the water column (Rigual-Hernández et al., 2020b).

2. Material and methods

2.1. Sample processing and biomarker analysis

The sediment trap samples collected at the SOTS observatory represent subsets of a series of long-term sediment trap deployments in the subantarctic waters south of Tasmania (Trull et al., 2001a; Wynn-Edwards et al., 2020). The samples were captured with three vertically-moored sediment traps of McLane PARFLUX-type design with a honeycomb baffle at the top (0.5 m^2 surface area), placed at 1000, 2000 and 3800 m depth in a water column of 4540 m. The trap sampling cups were filled with a buffered solution of sodium tetraborate (1 g L^{-1}), sodium chloride (5 g L^{-1}), strontium chloride (0.22 g L^{-1}), and mercury chloride (3 g L^{-1}). The 1000 and 2000 m sediment traps were equipped with 21 sampling cups with a sampling resolution of 16 days and sampled for a total of 336 days. Cup rotation intervals were synchronized between these two traps. The 3800 m trap was equipped with a 13-sample carousel, with a sample resolution of 26 days. The three time-series sediment traps completed their collection sequence as programmed without any instrumental failures providing a continuous time-series for 336 days for the 1000 and 2000 m sediment traps and 338 days for the 3800 m trap. Temperature was measured by a SBE56 sensor mounted at 45 m depth on a Pulse mooring (Trull et al., 2010). Further details of the field experiment and sample splitting can be found in Rigual-Hernández et al. (2020b). A total of 55 sediment trap samples were analysed. One fortieth of each of the sediment trap cup was used for biomarker analysis. Centrifuge tubes [PYREX® Bibby Sterilin, United Kingdom, 16 ∗ 100 mm; cleaned by sonication (Selecta, Spain) for 15 min using alkaline detergent at 5% (Extran AP13 at 5%, Merck Darmstadt, Germany) after each use], test tubes (PYREX® Corning, New York, 16 ∗ 100 mm) and chromatographic vials (Chromacol®, 1.1 mL) were used for the alkenone analyses after heated overnight at 400 °C. Solvents with quality for organic trace analysis (dichloromethane, hexane, methanol, toluene) and reagents (KOH, HCl, bis(trimethylsilyl) trifluoroacetamide –BSTFA-) were purchased from Merck (Darmstadt, Germany). The concentration of the heptatriaconta-8E,15E,22E-trie2-one and heptatriaconta-15E,22E-die2-one was determined using n-hexatriacontane (CH3(CH2)34CH3, 98%, Fluka) as internal standard.

For the removal of mercury chloride ($HgCl_2$) preservative, the supernatant was decanted and the last part of the supernatant was with a pipette to lose the minimum amount of sediment. Samples were washed with 2 × 10 mL of H_2O MQ to eliminate $HgCl_2$ by vortex agitation and centrifugation.

For the analysis of lipid organic compounds, the sediment samples were freeze-dried (12 h; Edwards High Vaccum International). The amount of dry sediment for analysis ranged from 2.1 to 74.6 mg (28.4 mg in average). Extraction was performed by sonication and vortex shaking, using 7.5 mL of dichloromethane (15 min; Selecta, Spain). The process was repeated three times to ensure that the extraction yield would be higher than 90%. The extracts were dried under nitrogen and hydrolysed with 10% potassium hydroxide in methanol to avoid interferences in detection and quantification of the compounds (2 mL; 12 h; room temperature). Extraction with hexane (2 mL; three times) yielded a fraction enriched in neutral compounds, which was cleaned with ultra-pure water. The purified extracts were derivatised with BSTFA (12 h; room temperature). Samples were injected diluted in toluene. They were analysed with a Varian gas chromatograph Model 450 equipped with a 1079 Programmable Temperature Vaporizing Injector (PTV) for cold on-column (sample volume 1ul, fast injection rate) and a Flame Ionization Detector (GC-FID; ceramic flame tip), temperature 320 °C, range 12). The instrument was equipped with a CPSIL-5 CB column coated with 100% dimethylsiloxane; film thickness of 0.12 um; L(m) ∗ ID (mm) ∗ OD(mm): 50 ∗ 0.32 ∗ 0.45. Hydrogen was the carrier gas (2.5 mL/min). Oven temperature was programmed from 90° (holding time of 1 min) to 170 °C at 20 °C/min, then to 280 °C at 6 °C/min (holding time 25 min), and finally, to 315 °C at 10 °C/min (holding time of 12 min). The injector was programmed from 90 °C (holding time of 0.5 min) to 310 °C at 200 °C/min (final holding time was 55 min). The acquisition programme was Thermo Atlas. Absolute concentration errors were below 10% and reproducibility tests showed that uncertainty in the $U^{K'}_{37}$ determinations was lower than 0.015 (ca. 0.5 °C).

2.2. Calculation of SST estimates from the alkenone measurements

A significant relationship between the alkenone unsaturation index $U^{K'}_{37}$ (expressed as $U^{K'}_{37} = C_{37:2} / (C_{37:2} + C_{37:3})$) and SSTs has been proven by a global core top analysis for all the oceans between the 60°N and the 60°S and from 0 to 29 °C (Müller et al., 1998), and also for global surface water calibration (Conte et al., 2006). However, documented variability across ocean regions has been attributed to several factors including: differences in the biogeographical distribution of the alkenone-producing organisms, varying growth rates, differences in seasonal production and/or differential preservation of alkenones, among others (Sikes et al., 1997; Conte et al., 2006; Tierney and Tingley, 2018; Max et al., 2020). Sikes and Volkman (1993) developed a regional calibration ($U^{K'}_{37}$ = 0.0414T–0.156) for the Southern Ocean that has proven to yield the most accurate temperature reconstructions in our study region (Sikes and Volkman, 1993; Ikehara et al., 1997; Sikes et al., 2005; Sikes et al., 2009; Sikes et al., 2019). Nonetheless, it is important to note that the use of the alkenone index U^{K}_{37}, which includes the $C_{37:4}$ in its calculation ($U^{K}_{37} = (C_{37:2} - C_{37:4}) / (C_{37:2} + C_{37:3} + C_{37:4})$), has been suggested to be a more suitable index for paleo SST reconstruction in the high latitude North Atlantic (Bard et al., 2000; Bendle and Rosell-Melé, 2004). In the subantarctic Southwest Pacific core top results show similar correlations for both indexes and although use of the U^{K}_{37} down-core returns colder temperatures and larger temperature changes (Ho et al., 2012) it remains uncertain if they are more accurate. Results from south of Tasmania, show a random relationship to temperature of the 37:4 alkenone (Sikes et al.,

1997). Therefore, here we compared the most commonly used calibrations of $U^{K'}_{37}$, i.e. Sikes and Volkman (1993), Müller et al. (1998), Conte et al. (2006) and the Bayesian B-spline regression model, BAYSPLINE, Tierney and Tingley (2018), with in situ SSTs measured at SOTS in order to determine which calibration and alkenone unsaturation index provides the greatest accuracy (see Section 2.4).

In order to estimate the annual integrated signature of the alkenone fluxes exported to the sea floor at SOTS, the annual flux-weighted $U^{K'}_{37}$ for each sediment trap record was estimated. The trap collection intervals encompassed periods shorter than a calendar year (336, 336 and 338 days at 1000, 2000 and 3800 m, respectively). Gaps in the record occurred during periods of minimum annual alkenone fluxes, therefore their influence on the annual estimates can be considered minute on the annual flux-weighted alkenone-derived temperature (~0.1 °C). Thus, while we focus the discussion on the collection interval estimates (i.e. data recorded during the sediment trap collection interval, i.e. 336 days for the 1000 and 2000 m traps and 338 days for the 3800 m trap), annualized estimates (i.e. fluxes estimated for 365 days assuming that particle flux outside of the collection period was equal to that of the last cup) can be considered essentially equivalent to those from the collection interval.

2.3. Physical, chemical and biological properties and NASA Ocean biogeochemistry model estimates at SOTS

In situ water temperature measurements were measured by a SBE56 sensor placed at 45 m depth (within the mixed layer) at SOTS (Rigual-Hernández et al., 2020b) while Sea Satellite-derived SST (°C) for the 142–143°E; 47–48°S region (one-degree grid) was obtained from NASAs sun-synchronous Moderate Resolution Imaging Spectroradiometer (MODIS-Aqua; 8-daily). Phosphate and total oxidised Nitrogen (NOx: nitrate plus nitrite) were measured from water samples collected at SOTS every 15 days previously published in Rigual-Hernández et al. (2020b) (Fig. 2b). Satellite-derived chlorophyll-*a* concentration for the SOTS region (one-degree grid: 142–143°E, 47–48°S) from August 2011 to July 2012 (8-daily) was obtained from MODIS-Aqua. Additionally, simulated coccolithophore concentration for the same region and time period were calculated with the NASA Ocean Biogeochemical Model (NOBM). The NOBM is a comprehensive and three-dimensional representation of circulation, biogeochemical and radiative processes in the global ocean (Gregg and Casey, 2007). The model assimilates SeaWiFS and MODIS total chlorophyll data and contains four major phytoplankton groups (diatoms, coccolithophores, cyanobacteria and chlorophytes), four nutrient groups, one herbivore group and three detrital pools. Both satellite-derived chlorophyll-*a* concentration and coccolithophore abundance estimates can be found in Fig. 2a.

2.4. Statistical analyses

The time lag between the SSTs and the traps was estimated by cross-correlating the daily in situ SSTs measured at 45 m at SOTS and the $U^{K'}_{37}$ daily values measured at the three sediment traps (e.g. Müller and Fischer, 2001; Müller and Fischer, 2003). The first three samples in the 1000 and 2000 m trap records and the first two in the 3800 m trap suggest anomalously high temperatures for winter 2011, showing

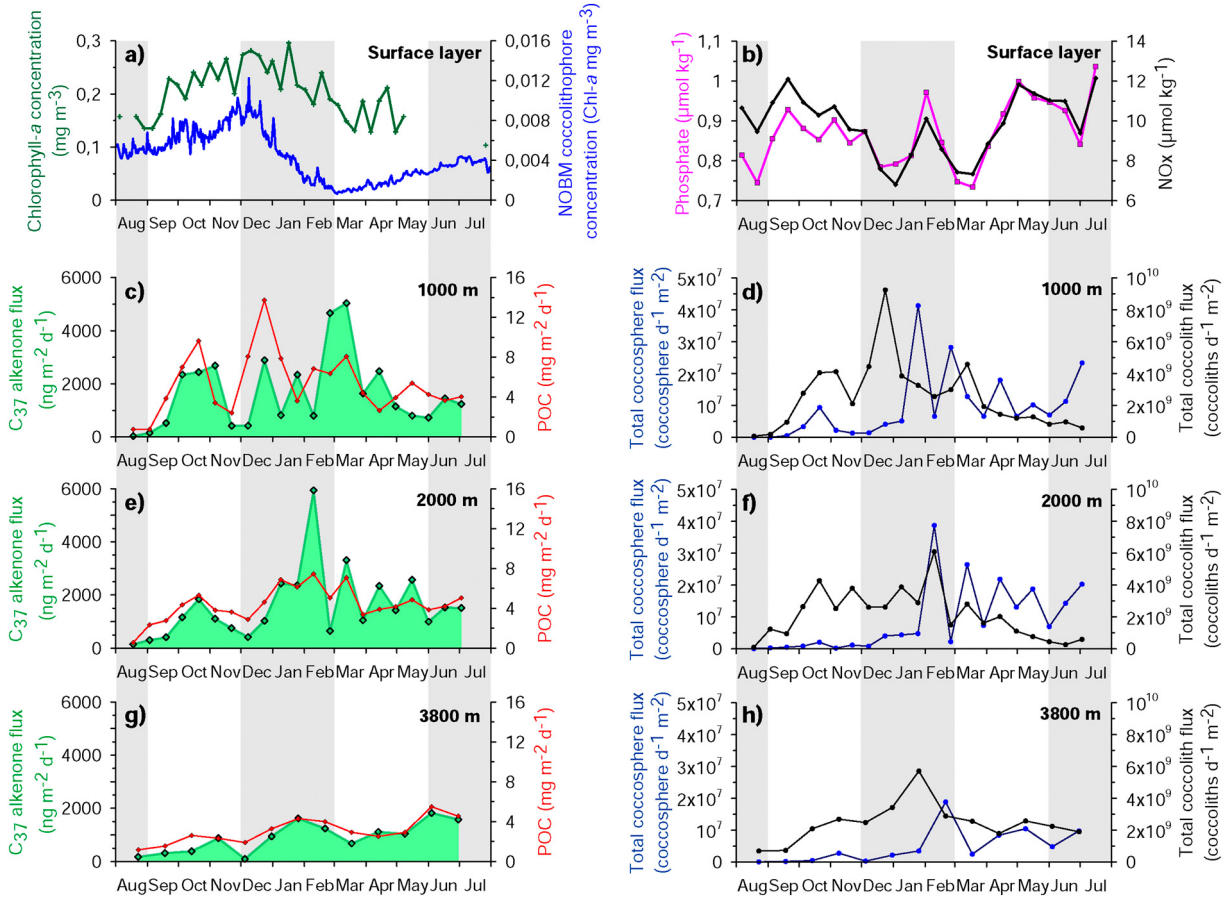

Fig. 2. (**a**) Satellite-derived chlorophyll-*a* concentration (MODIS-Aqua, 8-daily) and coccolithophore abundance (NOBM, daily) for the SOTS region (one-degree grid: 142–143°E; 44–45°S) from August 2011 to July 2012. (**b**) Phosphate and total oxidised nitrogen (NOx: nitrate plus nitrite) concentration measured at the SOTS site at 34 m depth (Rigual-Hernández et al., 2020b). (**c**, **e** and **g**) C_{37} alkenone (sum of $C_{37:2}$, $C_{37:3}$ and $C_{37:4}$) and Particulate Organic Carbon (POC; after Wynn-Edwards et al., 2020) fluxes. (**d**, **f** and **h**) Total coccolith and coccosphere fluxes at the 1000, 2000 and 3800 m traps from August 2011 to July 2012 (after Rigual-Hernández et al., 2020c). Shaded and non-shaded areas represent seasons: winter (JJA), spring (SON), summer (DJF) and autumn (MAM).

large deviations from the in situ SSTs (Fig. 3). The alkenone-derived temperatures suggested by these samples were considered to be substantially influenced by factors other than SST, and therefore were excluded from the cross-correlation analysis for estimation of alkenone sinking rates. It is important to note that the precision of the calculation of the sinking rates is limited by the duration of the sampling interval (i.e. 16 days for the 1000 and 2000 m traps and 26 days for the 3800 m trap) and therefore sinking rates calculated for this study represent a lower limit estimate.

The root mean square error (RMSE) between in situ SSTs measured at SOTS and alkenone-derived reconstructions applying Sikes and Volkman (1993), Müller et al. (1998) and Conte et al. (2006) calibrations using both $U^{K'}_{37}$ and U^{K}_{37} indexes was used to determine which calibration is most appropriate. Additionally, SSTs temperature reconstructions with $U^{K}_{37}{}'$ calibrated with BAYSPLINE (Tierney and Tingley, 2018) was also compared with in situ SST using RMSE analysis.

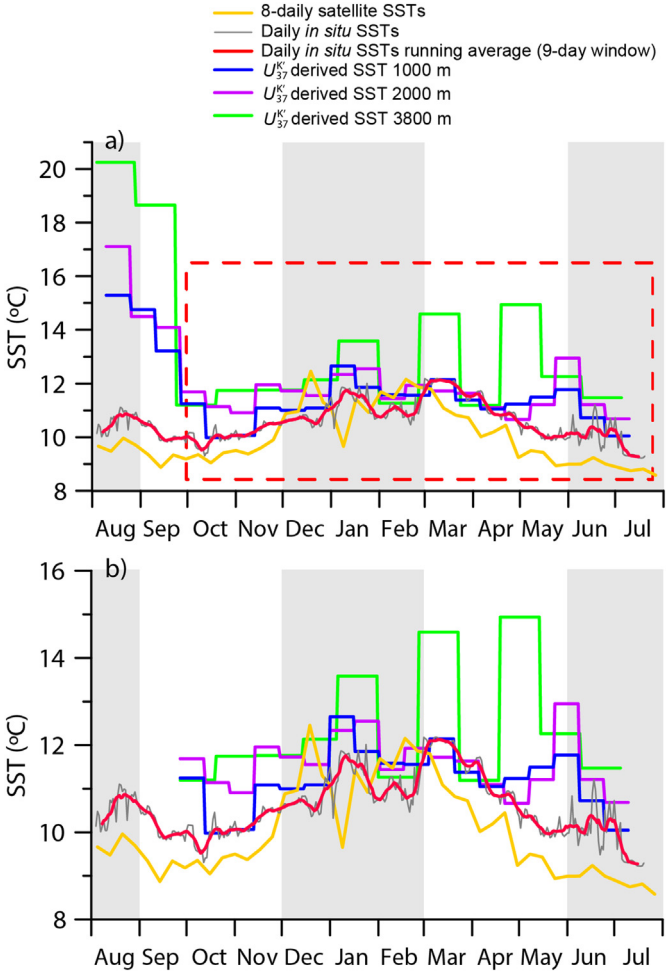

Fig. 3. Variability of SSTs and alkenone-derived reconstructions at SOTS from August 2011 to July 2012. (**a**) Satellite (8-daily) SST and in situ (daily) SST (°C) measured in the mixed layer (45 m) at the SOTS site and alkenone-derived SST reconstructions using the regional calibration of Sikes and Volkman (1993) applying the $U^{K'}_{37}$ index for the three sediment trap depths. (**b**) Satellite (8-daily) SST and in situ (daily) SST (°C) and alkenone-derived SST reconstructions zoomed into the period demarcated by the red dashed box in **a**. No time-lag was applied for the 1000 and 2000 m traps while a time lag of one week was applied for the 3800 m trap (see Table 1). Shaded and non-shaded areas represent seasons: winter (JJA), spring (SON), summer (DJF) and autumn (MAM).

3. Results and discussion

3.1. Alkenone production and export to the ocean interior

As evidenced from the shallowest 1000 m sediment trap, enhanced alkenone export starts in early October (>2000 ng m^{-2} d^{-1}; Fig. 2c). Relatively high fluxes are maintained through the first half of November – after which fluxes exhibit some excursions to low values (<1000 ng m^{-2} d^{-1}) until a second pulse in February through April (up to 5000 ng m^{-2} d^{-1} in March; Fig. 2c). During this 7-month interval almost 85% of the annual alkenone export occurs at 1000 m (Fig. 2c). The seasonal pattern of alkenone fluxes occurring in the 2000 and 3800 m traps shows substantial differences with that recorded in the 1000 m trap (Fig. 2e and g). Overall, the seasonal pattern of alkenone fluxes is smoothed with increasing depth (Fig. 2c, e and g), while the magnitude of the alkenone fluxes decrease towards the deeper layers of the water column (~560, 530 and 310 μg m^{-2} yr^{-1}, at 1000, 2000 and 3800 m, respectively). Despite these general trends, the 2000 m trap registered an alkenone flux peak in February earlier and of higher magnitude than that observed at 1000 m (Fig. 2c and e). There are several possible explanations for this, at first sight, counterintuitive observation that include (1) flux variations due to the wider particle source area potentially contributing to the sinking particle population collected by the deeper trap (Siegel et al., 1990; Siegel and Deuser, 1997), (2) under-sampling by the shallower trap, as quantified using radiogenic isotopes for traps moored at <1500 m water depth (Trull et al., 2001a; Yu et al., 2001), and/or (3) particle scavenging and biological repackaging in the mesopelagic zone (Conte et al., 2001; Conte et al., 2003; Lam and Marchal, 2015).

Seasonal changes of C_{37} alkenone fluxes (i.e. sum of $C_{37:2}$, $C_{37:3}$ and $C_{37:4}$ fluxes) were significantly correlated with both total coccosphere and total coccolith fluxes at the 1000 m ($r = 0.49$ and 0.52, respectively; $p < 0.05$, $n = 21$) and 2000 m traps ($r = 0.85$ and 0.62, respectively; $p < 0.05$, $n = 21$). These results evidence that, despite coccolithophores being exposed to different degradation processes in the water column that could potentially decouple their coccoliths from their organic content (e.g. grazing), these processes did not overwrite the overall relationships derived from the co-sedimentation of their inorganic and organic components (at least to 2000 m depth). It is likely that the geochemically labile alkenone compounds have been incorporated into sinking particles ballasted by hard components, such as coccoliths (Armstrong et al., 2002; Iversen and Ploug, 2010), thereby facilitating the rapid transfer of such bioreactive materials into the deep ocean (Conte et al., 2003). These relationships are weakest in the deepest trap ($r = 0.50$, $p > 0.05$ for the coccoliths and $r = 0.56$, $p < 0.05$ for the coccospheres, $n = 13$). Further degradation of algal aggregates, coccospheres and POC (particulate organic content) is likely to occur in the bathypelagic zone, which, together with the lower resolution of the 3800 m trap may explain the non-significant correlation in the deepest levels of the water column.

It is likely that the development of the coccolithophore bloom from September to November was limited due to competition with diatoms as suggested by enhanced BSi fluxes during this interval (Supplementary Fig. 1). Depletion of the winter silicate stocks in early-mid summer may have limited diatom production and export (Lannuzel et al., 2011; Rigual-Hernández et al., 2015; Eriksen et al., 2018) and this decrease in diatom abundance and export through resource limitation most likely allowed the development of a larger coccolithophore bloom in late summer (January to March) as evidenced by the maximum alkenones and coccosphere fluxes registered in the shallowest trap (Fig. 2c and d).

The delay between production in the upper water column and eventual export and collection by the sediment traps must be taken into consideration to estimate the exact timing of the production of the alkenones by the surface layer bloom. The cross-correlation analysis between the SSTs and the $U^{K'}_{37}$ registered in the traps suggests no statistically significant temporal lag for the 1000 and 2000 m trap records, while the highest significant correlation for the 3800 m trap was found for a lag of one week behind SSTs (Table 1). Thus, our observations suggest average annual

Table 1
Cross-correlation between daily in situ SSTs and daily alkenone unsaturation index $U^{K'}_{37}$ registered at the three sediment traps calculated for different lags. The first three samples of the 1000 and 2000 m trap and the first 2 samples of the 3800 m trap were removed from this analysis. Significant correlations (p value < 0.001) are set in **bold**. Asterisks (*) indicate the highest correlation coefficient for each sediment trap depth.

Sediment trap	Lag (weeks)						
	0	1	2	3	4	5	6
1000 m	**0.60***	**0.56**	**0.47**	**0.41**	**0.45**	**0.37**	**0.45**
2000 m	**0.28***	0.20	0.10	0.01	−0.03	−0.09	−0.02
3800 m	**0.31**	**0.43***	**0.39**	**0.32**	**0.25**	**0.26**	**0.37**

sinking rates ranging from 60 to 120 m d^{-1} (in particular, ~60, ~120 and ~120 m d^{-1} for the 1000, 2000 and 3800 m traps, respectively). The estimated sinking rates are consistent with the dominance of large particles observed in gel traps at SOTS (Ebersbach et al., 2011), are similar to those estimated by Closset et al. (2015) in the Polar Frontal Zone and Antarctic Zone waters south of Tasmania, and fall within the range of marine snow and fecal aggregates in the literature (10 to several hundreds m d^{-1}; Conte et al., 2001; Turner, 2002; Trull et al., 2008; Turner, 2015). It is worth noting that particle sinking rates have been documented to exhibit seasonal variations of an order of magnitude in the Southern Ocean, with lowest sinking rates during winter (down to <10 m d^{-1}) and highest during summer (>200 m d^{-1}) (Closset et al., 2015). Therefore, this seasonality should be kept in mind for the interpretation of our sediment trap records.

Thus, the period of maximum production of alkenones in the SAZ south of Tasmania appears to take place between October and April, i.e. spring to early autumn. This observation contrasts with seasonality suggested by the NASA Ocean Biogeochemical Model (NOBM) that predicts coccolithophore abundance (in Chl-*a* units) to increase from August to December 2011, declining to minimum annual values as early as January 2012 (austral midsummer; Fig. 2a). Thus, our observations urge caution when interpreting coccolithophore phenology in subantarctic waters based on NOBM simulations only. This is fully consistent with the evaluation of NOBM coccolithophore results by its creators, who noted that their abundance was controlled by multiple nutrient limitations and competition with other taxa making their prediction particularly difficult, and that while the model performed reasonably at global scale and particularly well in the North Atlantic, its performance was particularly poor in the Southern Ocean (Gregg and Casey, 2007).

3.2. Environmental controls on the seasonal variations of the alkenone derived SSTs

The Sikes and Volkman (1993) calibration yields the closest temperatures to the in situ SST of all calibrations in the upper water column (i.e. for the 1000 and 2000 m sediment trap records; Table 2) and has been proposed as the most accurate one for our study region (Sikes et al., 1997; Sikes et al., 2009; Sikes et al., 2019). Consequently, we use this regional calibration to interpret and discuss our results. It is important to note that our RMSE analysis indicates that although both alkenone-unsaturation indexes function in a similar fashion, U^{K}_{37} index is about 0.5 °C more accurate than the $U^{K'}_{37}$ in our sediment trap records (Table 2). These observations are in agreement with earlier work in the study region where both $U^{K'}_{37}$ and U^{K}_{37} have been showed to provide excellent results in paleo SST estimation at the region (Sikes et al., 1997; Martínez-Garcia et al., 2009; Ho et al., 2012). Although the accuracy of $U^{K'}_{37}$ is less than U^{K}_{37} overall, we find that during high flux times - the difference in accuracy between the two is greatly reduced relative to low flux periods. Sediment records overwhelmingly record the maximum export production periods. This information, combined with the fact that $C_{37:4}$ is not always measured, leads us to concentrate on the $U^{K'}_{37}$ relationship as this is more commonly found in the literature. Nonetheless, we also provide pertinent comparisons with the U^{K}_{37} index throughout the discussion.

Table 2
Root Mean Square Error (RMSE) in Celsius degrees between the in situ SSTs measured at SOTS and alkenone-derived SSTs with different calibrations using alkenone unsaturation indexes $U^{K'}_{37}$ (**a**) and U^{K}_{37} (**b**). The closest predictions are shown in bold. No time-lag was applied for the 1000 and 2000 m traps while a time lag of one week was applied for the 3800 m trap (see Table 1).

(a)

Sediment trap	Calibration			
	$U^{K'}_{37}$ Sikes and Volkman (1993)	$U^{K'}_{37}$ Conte et al. (2006)	$U^{K'}_{37}$ Müller et al. (1998)	$U^{K'}_{37}$ Tierney and Tingley (2018)
1000 m	**1.7**	2.1	2.6	3.1
2000 m	**2.2**	2.6	2.5	2.8
3800 m	4.0	4.3	3.6	**3.5**

(b)

Sediment trap	Calibration		
	U^{K}_{37} Sikes and Volkman (1993)	U^{K}_{37} Conte et al. (2006)	U^{K}_{37} Müller et al. (1998)
1000 m	**1.0**	1.3	2.9
2000 m	**1.6**	2.0	2.7
3800 m	**3.5**	3.9	**3.5**

At the onset of the record, i.e. August and September 2011, alkenone-based $U^{K'}_{37}$ SST reconstructions using the Sikes and Volkman (1993) calibration displayed large differences from the in situ SSTs of up to ~5, 6 and 10 °C warmer at 1000, 2000 and 3800 m, respectively (Fig. 3a). Since the representation of these large discrepancies overwhelm the seasonal signal in Fig. 3a for the rest of the year, alkenone-derived temperatures were replotted in Fig. 3b excluding August and September. After October 2011, the variation in alkenone-derived temperatures, roughly mirror the seasonal cycle of temperatures in the surface layer as suggested by our correlation analysis.

$U^{K'}_{37}$-derived temperatures from October 2011 ranged from 10° to 12.7 °C at 1000 m, 10.7° to 13 °C at 2000 m, and 11.2° to 14.9 °C at 3800 m (Fig. 3b), while the seasonal amplitude of temperature measured in situ in the surface layer for the same interval ranged between 9.2° to 12.2 °C (Fig. 3b). The offset between alkenone-derived temperatures and in situ SSTs for the same time interval was small, with deviations ranging between −0.3 and +1.7 °C at 1000 m. The alkenone-derived SSTs at 2000 and 3800 m sediment traps return warmer temperature estimates and, therefore, greater discrepancies, −0.4 to +2.9 °C and −0.1 to +4.4 °C, respectively (Fig. 3a and b).

We can take advantage of the existing physical and chemical measurements at the SOTS observatory together with coccolithophore flux data from the sediment traps to assess the influence of environmental and biological parameters on alkenone unsaturation. Laboratory experiments with *E. huxleyi* strains have demonstrated that nitrate and/or phosphate limitation (i.e. concentrations below 4 and 0.2 μM, respectively) can induce deviations of the $U^{K'}_{37}$ index (Epstein et al., 1998; Popp et al., 1998; Epstein et al., 2001), thereby yielding temperature reconstructions a few degrees colder than the actual water temperatures in which the *E. huxleyi* grew (Prahl et al., 2003; Sikes et al., 2005). Nutrient concentrations measured at the SOTS site (Fig. 2b) indicate that total oxidised nitrogen and phosphate concentrations during the study period were well above the threshold that might affect SST estimates. Values of phosphate and total oxidised nitrogen were always above ~7 and 0.7 μmol kg^{-1}, respectively (Fig. 2b). Based on these observations, nutrient stress can be discarded as a possible driver of the observed deviations of the alkenone-based temperature reconstructions from satellite and in situ SST estimates.

Low light levels have been observed to induce $U^{K'}_{37}$ values higher than the ambient water temperature in which *E. huxleyi* developed (Epstein et al., 2001; Prahl et al., 2003). Based on these studies, Sikes et al. (2005) concluded that slow growth rates under low light levels were the most likely driver of a similar winter deviation of the alkenone-derived

temperatures in sediment trap records in the nearby New Zealand sector of the SAZ. Indeed, during August and September, the deep winter mixing (up to 600 m, Rintoul and Trull, 2001) and seasonal thermocline breakdown could have enhanced winter low light stress by moving the phytoplankton below the critical depth for reasonable periods of time. Another possible explanation of the anomalously high temperature estimates at the onset of the record may lie in selective degradation of the more unsaturated alkenones when alkenone flux is low (winter) and the residence time is long resulting in an increase in the alkenone-derived temperatures (e.g. Rontani et al., 2008; Lee et al., 2011). During winter, the extremely deep convection of the water column and low particle sedimentation rates (possibly < 3 m d^{-1} as inferred from silicon isotopes in the nearby PFZ waters; Closset et al., 2015) could also have caused biogenic particles to remain in suspension in the SAZ water column for long periods of time. This could have exposed the alkenones produced during winter to prolonged biotic (e.g. bacterial hydrogenation) and/or abiotic (autoxidation) degradation processes (Rontani et al., 2008; Rontani et al., 2009; Rontani et al., 2013; Segev et al., 2016) compared to those particles produced during the productive spring-summer period. However, if selective degradation is affecting alkenones during winter, $C_{37:4}$ concentrations should be at their annual minima at the onset of the record at the three sediment trap depths, which is not the case (see Supplementary Table 1). While $C_{37:4}$ could be expected to be more abundant during the coldest months because of its association with colder temperatures (e.g. Brassell et al., 1986; Prahl and Wakeham, 1987; Prahl et al., 1988; Müller et al., 1998; Conte et al., 2006; Kitamura et al., 2018), the degradation hypothesis would imply a reduction of their concentrations through selective degradation compared to the $C_{37:2}$ and $C_{37:3}$ alkenones. The assessment of this hypothesis would require knowledge of the initial proportions of the different C_{37} alkenones in the surface layer during the winter months. Since this information is not available, the possibility of enhanced selective degradation of the more unsaturated alkenones during winter will remain hypothetical until examined by further research.

Based on the above, we infer that either light limitation on alkenone biosynthesis or selective degradation of the more unsaturated alkenones due to long particle exposure to degradation processes in the water column may have contributed to the large warm temperature estimate anomalies at the onset of the record. Regardless of the underlying cause, it is important to note that their effect on the total signal preserved in the sedimentary record is tiny, since alkenone production during August and September accounted for <5% of the annual alkenone flux to the seabed, as derived from the 1000 m trap. Another important consideration is that even under the hypothetical situation where both processes (i.e. light stress and selective degradation of alkenones) would have affected the alkenone unsaturation ratios simultaneously, they are unlikely to have been sufficient to explain the observed variability during winter. Batch culture experiments have shown that light stress can generate up to a 0.11 unit change in the $U^{K'}_{37}$ (Prahl et al., 2003), while field evidence indicates that $U^{K'}_{37}$ changes with increasing depth can contribute up to $+0.12$ units (Rontani et al., 2009). These values translate into a predicted 2.7 and 2.9 °C increase, respectively, in the inferred temperature when interpreted using the Sikes and Volkman (1993) calibration. Thus, taken together, they would account for only about half of the maximum deviation observed in the traps (i.e. ~10 °C). It follows that other factors aside from light stress and alkenone degradation must influence the alkenone unsaturation signal preserved in our sediment trap records.

3.3. Biological effects on the alkenone-based $U^{K'}_{37}$ index

We assessed the algal source of the alkenones in the SOTS traps to determine whether the alkenone-synthesizing populations (Volkman et al., 1995; Sawada et al., 1996; Conte et al., 1998; Versteegh et al., 2001) could account for the discrepancies between in situ SSTs alkenone-derived SSTs in our sediment trap records. Also, this analysis may help to explain the geographical variations in the alkenone-temperature relationship previously observed north and south of the Subtropical Front, in our study region (Sikes et al., 2009) and in the waters off New Zealand (Sikes et al., 2002; Sikes et al., 2019).

Changing proportions of *E. huxleyi* and *G. oceanica* have been suggested as a probable source of variability for the alkenone $U^{K'}_{37}$ index both in laboratory and field studies (Volkman et al., 1995; Sikes et al., 1997; Conte et al., 1998). Taxonomic analysis of the coccolith sinking assemblages collected by the traps at the SOTS observatory indicate that *E. huxleyi* largely dominated the assemblages during the collection period while *G. oceanica* displayed very low abundances (>80% and ≤1% of the annual flux-weighted assemblage at the three traps, respectively; Rigual-Hernández et al., 2020c). The negligible contribution of *G. oceanica* is supported by the ratio of C_{37} methyl alkenones to the total C_{38} methyl and ethyl alkenones, that averaged 1.24, 1.33 and 1.30 at the 1000, 2000 and 3800 m traps. This ratio has been reported to be decoupled with growth temperature and is substantially different between *E. huxleyi* (1.18–1.71, average 1.46) and *G. oceanica* (0.59–0.81, average 0.70) (Volkman et al., 1995). Although *G. oceanica* has an environmental preference for warmer waters, Findlay and Giraudeau (2000) did not report this species in the subtropical waters south of Tasmania, while its abundance in the subtropical sediments north of the Polar Front is very low (<5%; Findlay and Giraudeau, 2002). Therefore, based on the low abundance of *G. oceanica* in the STZ, it is unlikely that this species represents a driver of the differences between calibrations documented by Sikes et al. (2009) north and south of the Subtropical Front.

Notably, our correlation analysis revealed a strong relationship between the seasonal changes in the composition of the *E. huxleyi* populations and the temperature deviations between the alkenone-derived temperatures measured at the 1000 and 2000 m traps and in situ SSTs. There was a strong and positive correlation between changes in the relative abundance of *E. huxleyi* var. *huxleyi* (i.e. morphotype A and A o/c) in the shallower traps with the temperature deviation estimated with $U^{K'}_{37}$ index ($r = 0.59$ and 0.66 at 1000 and 2000 m, respectively; $p < 0.05$; Fig. 4). This indicates that high relative abundance of *E. huxleyi* var. *huxleyi* is associated with positive deviations from in situ SSTs, thereby implying an enhanced synthesis of $C_{37:2}$ alkenones relative to $C_{37:3}$ alkenones for the same growth conditions (Fig. 4). In turn, changes in the relative contribution of the morphotypes associated with ecotype *E. huxleyi* var. *aurorae* (i.e. B/C, C and B) are associated with reduced, and even slightly negative (down to -0.4 °C), deviations from in situ SSTs (Fig. 4). This suggests that at times of high relative abundance of *E. huxleyi* var. *aurorae* the proportion of $C_{37:3}$ relative to $C_{37:2}$ increases thereby yielding lower $U^{K'}_{37}$ index values, as also illustrated by the correlations between variety *aurorae* and the $U^{K'}_{37}$ index ($r = -0.59$ and -0.66 at 1000 and 2000 m, respectively; $p < 0.05$; Fig. 5). Notably, these relationships hold true, although with lower correlations, when the relative abundance of both *E. huxleyi* groups is compared with the U^{K}_{37} index (Fig. 5), suggesting that *E. huxleyi* var. *aurorae* may also produce higher proportions of $C_{37:4}$ than var. *huxleyi* for the same growth conditions. Since *E. huxleyi* var. *huxleyi* and *E. huxleyi* var. *aurorae* have been shown to be morphologically, physiologically, and genetically distinct (Cook et al., 2011; Cook et al., 2013), it is not unreasonable that they should display differences in the synthesis of alkenones in relation to temperature. Consequently, our data suggests that the endemic Southern Ocean ecotype *E. huxleyi* var. *aurorae* might produce a higher proportion of $C_{37:3}$ and $C_{37:4}$ relative to $C_{37:2}$ than the *E. huxleyi* var. *huxleyi*, a likely adaptation to cold water masses. This hypothesis is supported by earlier laboratory experiments that document differences between alkenone unsaturation indices and growth temperature across *E. huxleyi* strains (Conte et al., 1998). This can also explain the difference in temperature response found by Sikes and Volkman (1993) in the Southern Ocean calibration and the flattening of the response at cold temperatures. By this reasoning, as the proportion of Southern Ocean ecotype *E. huxleyi* var. *aurorae* increases, the local response to SST in alkenone unsaturation will move from the global to the regional calibration.

Changing proportions of the two *E. huxleyi* varieties were not significantly correlated with temperature deviations nor with the alkenone unsaturation indexes in the 3800 m sediment trap record (Figs. 4 and 5).

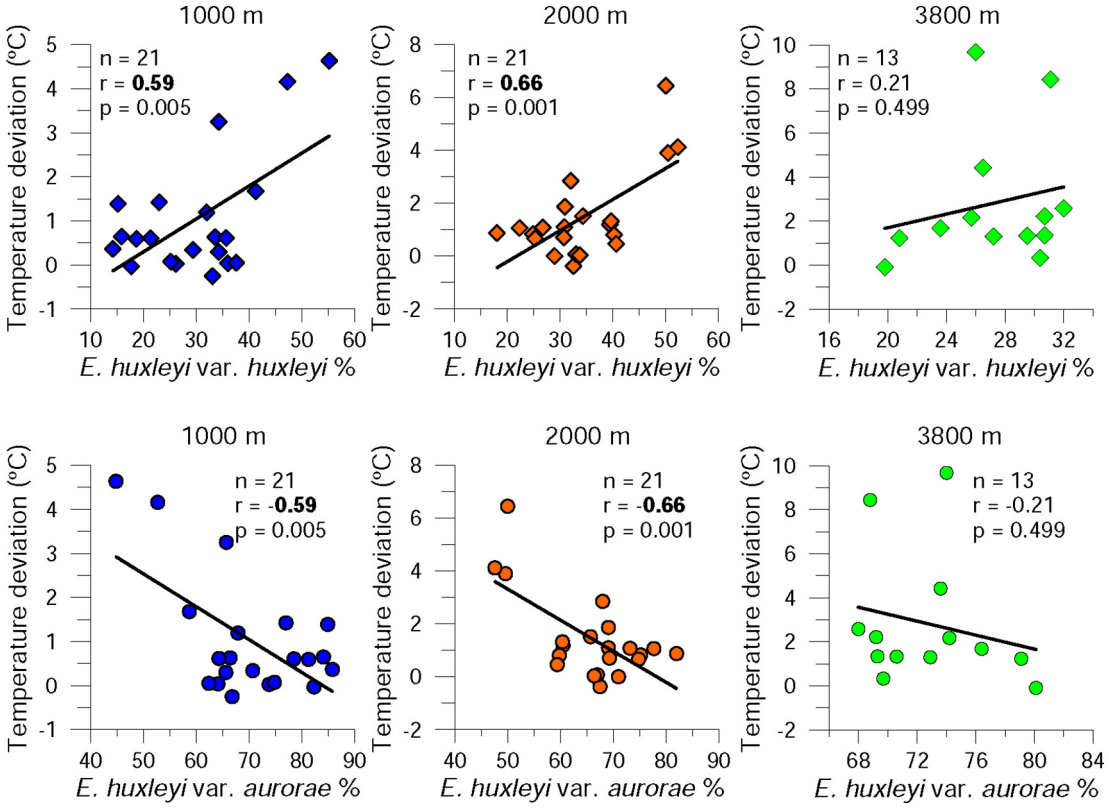

Fig. 4. Regression plots between the relative contribution (%) *E. huxleyi* var. *huxleyi* (type A and A o/c) and *E. huxleyi* var. *aurorae* (type B/C, C and B) with temperature deviations of alkenone-derived SSTs applying $U^{K'}_{37}$ index to Sikes and Volkman (1993) calibration and in situ SSTs at the three sediment trap depths. A delay of one week was applied for the comparison of the 3800 m trap (see text). Correlations in **bold** are significant at $p < 0.05$.

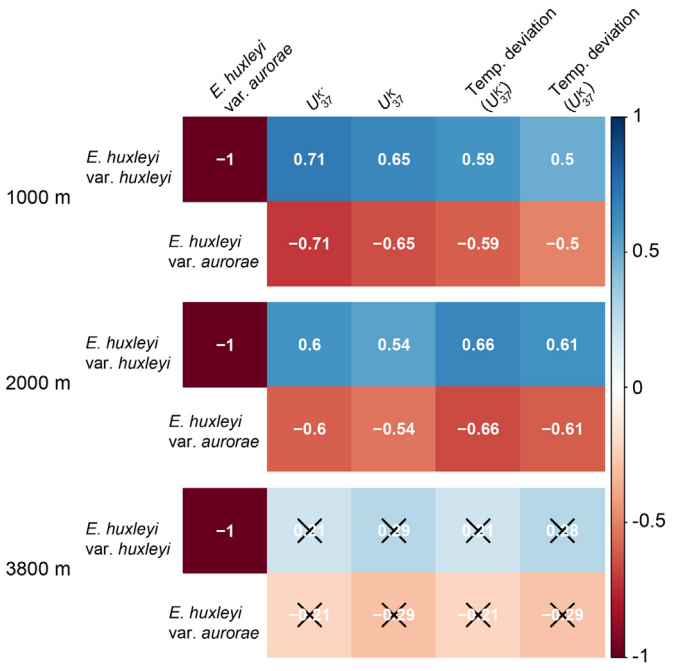

Fig. 5. Pearson correlations between *E. huxleyi* varieties and temperature deviations of alkenone-derived temperatures estimated with Sikes and Volkman (1993) calibration using both $U^{K'}_{37}$ and U^{K}_{37} and alkenone unsaturation indexes. Non-significant correlations (p values > 0.05) are crossed out. $n = 21$ samples for the 1000 and 2000 m traps and $n = 13$ for the 3800 m trap.

Several factors may have caused the blurring of the correlation in the deepest trap: (1) the lower sample size of the 3800 trap (13 samples versus 21 for the 1000 and 2000 m traps), (2) differing influence of particle scavenging and repackaging by zooplankton on the organic content and coccoliths at bathypelagic depths and/or (3) the preferential decomposition of tetra- and triunsaturated alkenones in the water column.

Lastly, it is worth noting that the correlation between temperature deviations and *E. huxleyi* varieties become not significant if winter samples, identified earlier as predicting anomalously high SST values, are excluded from the correlation (e.g., $r = -0.03$ between *E. huxleyi* var. *huxleyi* and temperature deviation at 1000 m, $n = 18$). This suggests that morphotypes are not a very strong control on the $U^{K'}_{37}$ index in the productive season. The Sikes and Volkman (1993) calibration was based on water samples retrieved on different cruises in October and November. Therefore, a null discrepancy between alkenone-derived SSTs and in situ SSTs - and the lack of correlation between temperature deviations and *E. huxleyi* assemblage composition - would be expected when the proportion of *E. huxleyi* morphotypes are similar to those present in the water samples used for the calibration. Following this reasoning, it is logical that the largest discrepancies between in situ and alkenone-predicted SSTs are observed during winter 2011, the period characterized by the highest annual relative contributions of *E. huxleyi* var. *huxleyi* (Supplementary Fig. 2) which is the most different from those used in the Sikes and Volkman (1993) calibration. Another possible explanation is that the role of *E. huxleyi* var. *huxleyi* in altering the alkenone-SST relationships may stem from multiple causes including transport from more northerly sources, differences in alkenone synthesis, and propensity for alteration.

3.4. Changes of the alkenone-based $U^{K'}_{37}$ index with depth in the water column

Annual flux-weighted alkenone reconstructions in the 1000 m trap suggest a mean temperature record of 11.3 °C using the $U^{K'}_{37}$ index (Table 3).

Table 3
a) Satellite SST climatology for the region 142–143°E; 47–48°S (2002 – 2020) and in situ SST measurements at the SOTS site (45 m depth). b) Alkenone based-SST reconstructions during the sediment trap collection intervals and annualized values with the Sikes and Volkman (1993) calibration using $U^{K'}_{37}$ and U^{K}_{37} indexes. c) Alkenone-based SST reconstructions for sediment core-top GC017 with the Sikes and Volkman (1993) calibration using $U^{K'}_{37}$ after Sikes et al. (2009).

(a)

Surface layer SSTs (°C)	Satellite SST climatology	In situ SSTs at SOTS
Annual average	10.0	10.6
Summer months (Dec, Jan and Feb)	11.1	11.0
Alkenone production (Sep to Mar, 7 months)	10.3	10.9

(b)

Sediment trap annual SST estimates (°C)	Sikes and Volkman (1993) calibration			
	Collection interval		Annualized estimate	
	$U^{K'}_{37}$	U^{K}_{37}	$U^{K'}_{37}$	U^{K}_{37}
1000 m	11.3	11.0	11.2	10.9
2000 m	11.6	11.2	11.6	11.1
3800 m	12.7	12.1	12.6	12.0

(c)

	$U^{K'}_{37}$ Sikes and Volkman (1993)
SST estimates from coretop GC17 (°C)	13.0

This is, within the average error of our measurements (1.7 °C, Table 2), the same as the annual average temperature for the surface layer at SOTS (i.e. 10.6 °C). Annual alkenone reconstructions increased with increasing depth, suggesting annual temperatures of 11.6 °C at 2000 m and 12.7 °C at 3800 m (Table 3). Notably, the annual temperature estimated from the deepest sediment trap is almost identical to that derived from the nearby sea-bed sediments of core-top GC17 (13 °C; Sikes et al., 2009).

Two hypotheses can be considered to explain the enlarging discrepancy with increasing depth in the water column: lateral advection and/or selective degradation of alkenones; we discuss both possibilities below. Tamsitt et al. (2019) recently documented that a branch of the deep eastern Indian Ocean boundary flows poleward into the ACC southwest of Tasmania (Fig. 1). This deep current (~1500 to 3000 m depth) transports a substantial amount of water (0.8 Sverdrups) from the Indian and Pacific basins, carrying carbon- and nutrient-rich deep waters into the Subantarctic Zone. Thus, it could be argued that the apparently warm signal recorded by alkenones in the 3800 m traps could be due to a contribution of alkenones produced in the warmer subtropical waters and laterally advected into the SOTS region. However, the similar composition of *E. huxleyi* morphotypes at the three trap depths (Supplementary Fig. 2) and the overwhelming dominance of morphotype B/C, strongly suggests that the bulk of the coccoliths flux to the traps is of autochthonous origin. This statement is supported by the diatom assemblage collected by the 3800 m trap that is characteristic of the SAZ (Rigual-Hernández et al., 2016). These results are not contradictory since fine-grained organic matter can be selectively transported by currents for long distances (e.g. Mollenhauer et al., 2003; Eglinton and Eglinton, 2008), while calcareous and siliceous microplankton settle faster due to their greater grain size and ballasting effect on organic aggregates (Armstrong et al., 2002; Ziveri et al., 2007; De La Rocha et al., 2008). In the SOTS region, the bulk of the particles sinking out of the mixed layer are in the form of fecal-aggregates (Ebersbach et al., 2011) which are intrinsically characterized by high sinking rates (Turner, 2002; Turner, 2015). Additionally, previous research in the SOTS sediment traps indicates that lithogenic material makes a negligible contribution (<1%) to the total mass flux at the three depths (Trull et al., 2001a). Thus, while the advective inputs of small particles from the subtropical region may occur (Wynn-Edwards et al., 2020), evidence from this study indicates that the bulk of the alkenones exported to the deep ocean are of subantarctic origin (this does not exclude the possibility that the very low winter fluxes samples were derived from sources further north).

Preferential degradation of $C_{37:3}$ versus $C_{37:2}$ alkenones throughout the water column could also account for the $U^{K'}_{37}$ variations with increasing depth particularly in periods of reduced production. Indeed, the magnitude of the maximum POC and C_{37} alkenone fluxes decreased four and two-fold, respectively, between 2000 and 3800 m, evidencing substantial remineralization of organic matter in the lower half of the water column (Fig. 2 and Supplementary Fig. 1). Conte et al. (2006) documented that differences between modern satellite estimates and alkenone-based SSTs increased towards polar latitudes and proposed that this offset could be attributed to differences in the degradation of $C_{37:3}$ versus $C_{37:2}$ alkenones in the water column and/or in the surface sediments. Autooxidation of alkenones and bacterial remineralization have been reported to selectively degrade the more unsaturated alkenones, inducing a change in the unsaturation ratio thereby producing a warm temperature bias (Rontani et al., 2005; Rontani et al., 2008; Rontani et al., 2013). Given that degradation processes are often retarded by colder temperatures, this enhanced degradation would need to involve food web or residence time differences that are not yet understood (and are beyond the scope of the present study). Based on all the above, any/or a combination of the mentioned degradation processes in the water column might be responsible for the changes in the alkenone index $U^{K'}_{37}$ with increasing depth.

3.5. Possible influence of *Emiliania huxleyi* ecotypes on the alkenone-based $U^{K'}_{37}$ index

The strong correlations between the presence of different *E. huxleyi* varieties and the $U^{K'}_{37}$ suggest that the makeup of the alkenone-synthesizing populations could help to explain the discrepancies between global and regional calibrations north and south of the Subtropical Front previously noted by Sikes et al. (2009). Indeed, we speculate that the influence of the composition of *E. huxleyi* populations could be particularly significant for alkenone-based reconstructions in the subtropical-subantarctic transition where the Antarctic Circumpolar Current acts as an important open-ocean barrier for gene flow between plankton populations (Cook et al., 2013). The biogeographical distribution of these *E. huxleyi* varieties is clearly reflected in the water column of the Southern Ocean, where types A and A o/c are abundant in the subtropical waters while B/C increases its abundance south of the Subtropical Front, largely dominating coccolithophore assemblages in the colder waters (Findlay and Giraudeau, 2000; Cubillos et al., 2007; Mohan et al., 2008; Patil et al., 2014; Saavedra-Pellitero and Baumann, 2015; Rigual-Hernández et al., 2020a; Rigual-Hernández et al., 2020b). It follows that the pronounced differences of *E. huxleyi* ecological varieties north versus south of the Subtropical Front could be partially, if not largely, responsible for the anomalies in predictions of sea surface temperature (SST) in the subtropical and subantarctic sediments of the Southern Ocean. Importantly, the relationship between alkenone index $U^{K'}_{37}$ and growth temperature has not yet been tested – to the best of our knowledge – on any strain of the endemic Southern Ocean ecotype *E. huxleyi* var. *aurorae* (Cook et al., 2011). Therefore, physiological response experiments under controlled temperature conditions with *E. huxleyi* var. *aurorae* strains are crucially needed to assess the influence of genetic variability in the alkenone vs. temperature relationship and consequent effects on the calibration of alkenone-based temperature estimates in the Southern Ocean.

4. Conclusions

Our data suggests that in the subantarctic Southern Ocean, the long exposure to water column degradation processes, associated with transit to the deepest levels of the water column, increases ca. 2 °C the discrepancy between annual alkenone-based temperature reconstructions and annual instrumentally measured SST. Evidence suggests that these temperature deviations are most likely due to selective degradation of the more

unsaturated alkenones. Moreover, comparison of different calibrations with SSTs measured in situ at SOTS indicates that the regional calibration of Sikes and Volkman (1993) produces the most accurate temperature reconstructions. Notably, seasonal changes in the *E. huxleyi* assemblage in the 1000 and 2000 m sediment trap records are strongly correlated with deviations of the alkenone paleothermometer from in situ SSTs. Notably, seasonal changes in the *E. huxleyi* assemblage in the 1000 and 2000 m sediment trap records are strongly correlated with deviations of the alkenone paleothermometer from in situ SSTs. It follows that the substantial variations in the relative abundance of *E. huxleyi* ecotypes north and south of the Subtropical Front could represent the underlying reason for the distortion in the alkenone-based SST reconstructions in the Southern Ocean when using global calibrations. However, it is important to note that the significance of the observed correlations is largely determined by the samples collected during the non-productive period (i.e., winter). This observation suggests that other factors such as long residence time in the water column and enhanced selective degradation of the most unsaturated alkenones could also account for the observed deviations of the alkenone paleothermometer at the SOTS site. The assessment of the possible role of the composition of *E. huxleyi* assemblages on the $U^{K'}_{37}$ requires laboratory culture of Southern Ocean strains of *E. huxleyi* var. *aurorae* under different temperatures. If these analyses corroborate that the relationship between the ratio of di- to triunsaturated methyl alkenones and growth temperatures is different for *E. huxleyi* var. *aurorae* and *E. huxleyi* var. *huxleyi*, the identification of *E. huxleyi* morphotypes in the analysed material will be necessary to improve the accuracy of the alkenone paleothermometer in subpolar ecosystems.

Supplementary data to this article can be found online at https://doi.org/10.1016/j.scitotenv.2021.152474.

Author contributions

TWT, DMD and RSE planned and performed the field experiment. ARH, TWT, JAF, FJS, SN, TR and FA conceived the project and facilitated acquisition of the financial support for the project leading to this publication. NB and BM performed biogeochemical analyses. JMSS and ARH performed numerical analyses. The paper was written by ARH with input from all authors. All authors approved the final version of the manuscript.

Declaration of competing interest

The authors declare that they have no known competing financial interests or personal relationships that could have appeared to influence the work reported in this paper.

Acknowledgments

We thank the constructive comments and suggestions of five anonymous reviewers that helped improve and clarify this paper. Cathryn Wynn-Edwards (IMAS) provided support in sample splitting/processing and laboratory analysis. We are grateful to Ivia Closset for helpful comments on interpretation of results and to Erik Behrens for providing data for this research. This project has received funding from the European Union's Horizon 2020 research and innovation programme under the Marie Skłodowska-Curie grant agreement number 748690 – SONAR-CO2. Australia's Integrated Marine Observing System (IMOS) is enabled by the National Collaborative Research Infrastructure Strategy (NCRIS). It is operated by a consortium of institutions as an unincorporated joint venture, with the University of Tasmania as Lead Agent. This study was supported by the Spanish Ministerio de Economía y Competitividad Project CGL2015-68459-P. The Severo Ochoa Grant CEX2018-000794-S funded by MCIN/AEI/10.13039/501100011033 is likewise acknowledged. This study received Portuguese national funds from FCT - Foundation for Science and Technology through project UIDB/04326/2020, and from the operational programmes CRESC Algarve 2020 and COMPETE 2020 through projects EMBRC.PT ALG-01-0145-FEDER-022121 and EMSO-PT POCI-01-0145-FEDER-022157. Argo data were collected and made freely available by the International Argo Program and the national programmes that contribute to it. (http://www.argo.ucsd.edu, http://argo.jcommops.org). The Argo Program is part of the Global Ocean Observing System. Satellite SST, chlorophyll-*a* and coccolithophore concentration (NOBM) data sets were produced with the Giovanni online data system, developed and maintained by the NASA GES DISC.

References

Armstrong, R.A., Lee, C., Hedges, J.I., Honjo, S., Wakeham, S.G., 2002. A new, mechanistic model for organic carbon fluxes in the ocean based on the quantitative association of POC with ballast minerals. Deep-Sea Res. II Top. Stud. Oceanogr. 49, 219–236.

Bard, E., Rostek, F., Turon, J.-L., Gendreau, S., 2000. Hydrological impact of Heinrich events in the subtropical Northeast Atlantic. Science 289, 1321–1324.

Behrens, E., Hogg, A.M., England, M.H., Bostock, H., 2021. Seasonal and interannual variability of the subtropical front in the New Zealand region. J. Geophys. Res. Oceans 126, e2020JC016412.

Belkin, I.M., Gordon, A.L., 1996. Southern Ocean fronts from the Greenwich meridian to Tasmania. J. Geophys. Res. Oceans 101, 3675–3696.

Bendle, J., Rosell-Melé, A., 2004. Distributions of UK37 and UK37′ in the surface waters and sediments of the Nordic Seas: Implications for paleoceanography. Geochem. Geophys. Geosyst. 5.

Boon, J.J., de Leeuw, J.W., 1979. The analysis of wax esters, very long mid-chain ketones and sterol ethers isolated from Walvis Bay diatomaceous ooze. Mar. Chem. 7, 117–132.

Brassell, S., Eglinton, G., Marlowe, I., Pflaumann, U., Sarnthein, M., 1986. Molecular stratigraphy: a new tool for climatic assessment. Nature 320, 129–133.

Closset, I., Cardinal, D., Bray, S.G., Thil, F., Djouraev, I., Rigual-Hernández, A.S., Trull, T.W., 2015. Seasonal variations, origin, and fate of settling diatoms in the Southern Ocean tracked by silicon isotope records in deep sediment traps. Glob. Biogeochem. Cycles 29, 1495–1510.

Conte, M.H., Thompson, A., Eglinton, G., Green, J.C., 1995. Lipid biomarker diversity in the coccolithophorid EMILIANIA huxleyi (PRYMNESIOPHYCEAE) and the related species gephyrocapsa OCEANICA1. J. Phycol. 31, 272–282.

Conte, M.H., Thompson, A., Lesley, D., Harris, R.P., 1998. Genetic and physiological influences on the Alkenone/Alkenoate versus growth temperature relationship in Emiliania huxleyi and gephyrocapsa oceanica. Geochim. Cosmochim. Acta 62, 51–68.

Conte, M.H., Ralph, N., Ross, E.H., 2001. Seasonal and interannual variability in deep ocean particle fluxes at the oceanic flux program (OFP)/Bermuda Atlantic time series (BATS) site in the western Sargasso Sea near Bermuda. Deep-Sea Res. II Top. Stud. Oceanogr. 48, 1471–1505.

Conte, M., Dickey, T., Weber, J., Johnson, R., Knap, A., 2003. Transient physical forcing of pulsed export of bioreactive material to the deep Sargasso Sea. Deep-Sea Res. I Oceanogr. Res. Pap. 50, 1157–1187.

Conte, M.H., Sicre, M.-A., Rühlemann, C., Weber, J.C., Schulte, S., Schulz-Bull, D., Blanz, T., 2006. Global temperature calibration of the alkenone unsaturation index (UK′37) in surface waters and comparison with surface sediments. Geochem. Geophys. Geosyst. 7.

Cook, S.S., Whittock, L., Wright, S.W., Hallegraeff, G.M., 2011. Photosynthetic pigment and genetic differences between two southern ocean morphotypes of Emiliania huxleyi (haptophyta). J. Phycol. 47, 615–626.

Cook, S.S., Jones, R.C., Vaillancourt, R.E., Hallegraeff, G.M., 2013. Genetic differentiation among australian and Southern Ocean populations of the ubiquitous coccolithophore Emiliania huxleyi (Haptophyta). Phycologia 52, 368–374.

Cubillos, J., Wright, S., Nash, G., De Salas, M., Griffiths, B., Tilbrook, B., Poisson, A., Hallegraeff, G., 2007. Calcification morphotypes of the coccolithophorid Emiliania huxleyi in the Southern Ocean: changes in 2001 to 2006 compared to historical data. Mar. Ecol. Prog. Ser. 348, 47–54.

De La Rocha, C.L., Nowald, N., Passow, U., 2008. Interactions between diatom aggregates, minerals, particulate organic carbon, and dissolved organic matter: further implications for the ballast hypothesis. Glob. Biogeochem. Cycles 22.

Deacon, G.E.R., 1982. Physical and biological zonation in the Southern Ocean. Deep Sea Res. A. Oceanogr. Res. Pap. 29, 1–15.

Ebersbach, F., Trull, T.W., Davies, D.M., Bray, S.G., 2011. Controls on mesopelagic particle fluxes in the sub-Antarctic and polar frontal zones in the Southern Ocean south of Australia in summer—Perspectives from free-drifting sediment traps. Deep-Sea Res. II Top. Stud. Oceanogr. 58, 2260–2276.

Eglinton, T.I., Eglinton, G., 2008. Molecular proxies for paleoclimatology. Earth Planet. Sci. Lett. 275, 1–16.

Eltgroth, M.L., Watwood, R.L., Wolfe, G.V., 2005. Production and cellular localization of neutral long-chain lipids in the haptophyte algae isochrysis galbana and emiliania huxleyi 1. J. Phycol. 41, 1000–1009.

Epstein, B.L., D'Hondt, S., Quinn, J.G., Zhang, J., Hargraves, P.E., 1998. An effect of dissolved nutrient concentrations on alkenone-based temperature estimates. Paleoceanography 13, 122–126.

Epstein, B.L., D'Hondt, S., Hargraves, P.E., 2001. The possible metabolic role of C37 alkenones in emiliania huxleyi. Org. Geochem. 32, 867–875.

Eriksen, R., Trull, T.W., Davies, D., Jansen, P., Davidson, A.T., Westwood, K., van den Enden, R., 2018. Seasonal succession of phytoplankton community structure from autonomous sampling at the australian Southern Ocean time series (SOTS) observatory. Mar. Ecol. Prog. Ser. 589, 13–31.

Findlay, C.S., Giraudeau, J., 2000. Extant calcareous nannoplankton in the australian sector of the Southern Ocean (austral summers 1994 and 1995). Mar. Micropaleontol. 40, 417–439.

Findlay, C.S., Giraudeau, J., 2002. Movement of oceanic fronts south of Australia during the last 10 ka: interpretation of calcareous nannoplankton in surface sediments from the Southern Ocean. Mar. Micropaleontol. 46, 431–444.
Gregg, W.W., Casey, N.W., 2007. Modeling coccolithophores in the global oceans. Deep-Sea Res. II Top. Stud. Oceanogr. 54, 447–477.
Harada, N., Sato, M., Shiraishi, A., Honda, M.C., 2006. Characteristics of alkenone distributions in suspended and sinking particles in the northwestern North Pacific. Geochim. Cosmochim. Acta 70, 2045–2062.
Herbert, T.D., 2001. Review of alkenone calibrations (culture, water column, and sediments). Geochem. Geophys. Geosyst. 2.
Ho, S.L., Mollenhauer, G., Lamy, F., Martínez-Garcia, A., Mohtadi, M., Gersonde, R., Hebbeln, D., Nunez-Ricardo, S., Rosell-Melé, A., Tiedemann, R., 2012. Sea surface temperature variability in the Pacific sector of the Southern Ocean over the past 700 kyr. Paleoceanography 27.
Ikehara, M., Kawamura, K., Ohkouchi, N., Kimoto, K., Murayama, M., Nakamura, T., Oba, T., Taira, A., 1997. Alkenone Sea surface temperature in the Southern Ocean for the last two deglaciations. Geophys. Res. Lett. 24, 679–682.
Iversen, M.H., Ploug, H., 2010. Ballast minerals and the sinking carbon flux in the ocean: carbon-specific respiration rates and sinking velocity of marine snow aggregates. Biogeosciences 7, 2613–2624.
Jaraula, C.M.B., Brassell, S.C., Morgan-Kiss, R.M., Doran, P.T., Kenig, F., 2010. Origin and tentative identification of tri to pentaunsaturated ketones in sediments from Lake fryxell, East Antarctica. Org. Geochem. 41, 386–397.
Kitamura, E., Kotajima, T., Sawada, K., Suzuki, I., Shiraiwa, Y., 2018. Cold-induced metabolic conversion of haptophyte di- to tri-unsaturated C37 alkenones used as palaeothermometer molecules. Sci. Rep. 8, 2196.
Kopczynska, E.E., Dehairs, F., Elskens, M., Wright, S., 2001. Phytoplankton and microzooplankton variability between the subtropical and polar fronts south of Australia: thriving under regenerative and new production in late summer. Journal of Geophysical Research: Oceans 106, 31597–31609.
Krueger-Hadfield, S., Balestreri, C., Schroeder, J., Highfield, A., Helaouët, P., Allum, J., Moate, R., Lohbeck, K.T., Miller, P., Riebesell, U., 2014. Genotyping an emiliania huxleyi (Prymnesiophyceae) bloom event in the North Sea reveals evidence of asexual reproduction. Biogeosciences 11, 5215–5234.
Lam, P.J., Marchal, O., 2015. Insights into particle cycling from thorium and particle data. Annu. Rev. Mar. Sci. 7, 159–184.
Lannuzel, D., Bowie, A.R., Remenyi, T., Lam, P., Townsend, A., Ibisanmi, E., Butler, E., Wagener, T., Schoemann, V., 2011. Distributions of dissolved and particulate iron in the sub-Antarctic and polar frontal Southern Ocean (Australian sector). Deep-Sea Res. II Top. Stud. Oceanogr. 58, 2094–2112.
Lee, K.E., Khim, B.-K., Otosaka, S., Noriki, S., 2011. Sediment trap record of alkenones from the East Sea (Japan Sea). Org. Geochem. 42, 255–261.
Liu, Z., Pagani, M., Zinniker, D., DeConto, R., Huber, M., Brinkhuis, H., Shah, S.R., Leckie, R.M., Pearson, A., 2009. Global cooling during the eocene-oligocene climate transition. Science 323, 1187–1190.
López, J.F., Grimalt, J.O., 2004. Phenyl- and cyclopentylimino derivatization for double bond location in unsaturated C37–C40 alkenones by GC-MS. J. Am. Soc. Mass Spectrom. 15, 1161–1172.
Malinverno, E., Triantaphyllou, M.V., Dimiza, M.D., 2015. Coccolithophore assemblage distribution along a temperate to polar gradient in the West Pacific sector of the Southern Ocean (January 2005). Micropaleontology 61, 489–506.
Martínez-Garcia, A., Rosell-Melé, A., Geibert, W., Gersonde, R., Masqué, P., Gaspari, V., Barbante, C., 2009. Links between iron supply, marine productivity, sea surface temperature, and CO2 over the last 1.1 ma. Paleoceanography 24.
Martrat, B., Grimalt, J.O., Shackleton, N.J., de Abreu, L., Hutterli, M.A., Stocker, T.F., 2007. Four climate cycles of recurring deep and surface water destabilizations on the iberian margin. Science 317, 502–507.
Max, L., Lembke-Jene, L., Zou, J., Shi, X., Tiedemann, R., 2020. Evaluation of reconstructed sea surface temperatures based on U37k′ from sediment surface samples of the North Pacific. Quat. Sci. Rev. 243, 106496.
Mohan, R., Mergulhao, L.P., Guptha, M.V.S., Rajakumar, A., Thamban, M., AnilKumar, N., Sudhakar, M., Ravindra, R., 2008. Ecology of coccolithophores in the indian sector of the Southern Ocean. Mar. Micropaleontol. 67, 30–45.
Mollenhauer, G., Eglinton, T.I., Ohkouchi, N., Schneider, R.R., Müller, P.J., Grootes, P.M., Rullkötter, J., 2003. Asynchronous alkenone and foraminifera records from the Benguela upwelling system. Geochim. Cosmochim. Acta 67, 2157–2171.
Müller, P.J., Fischer, G., 2001. A 4-year sediment trap record of alkenones from the filamentous upwelling region off cape blanc, NW Africa and a comparison with distributions in underlying sediments. Deep-Sea Res. I Oceanogr. Res. Pap. 48, 1877–1903.
Müller, P.J., Fischer, G., 2003. C 37-alkenones as paleotemperature tool: fundamentals based on sediment traps and surface sediments from the South Atlantic Ocean. The South Atlantic in the Late Quaternary. Springer, pp. 167–193.
Müller, P.J., Kirst, G., Ruhland, G., Von Storch, I., Rosell-Melé, A., 1998. Calibration of the alkenone paleotemperature index U 37 K′ based on core-tops from the eastern South Atlantic and the global ocean (60 N-60 S). Geochim. Cosmochim. Acta 62, 1757–1772.
Müller, M.N., Trull, T.W., Hallegraeff, G.M., 2015. Differing responses of three Southern Ocean emiliania huxleyi ecotypes to changing seawater carbonate chemistry. Mar. Ecol. Prog. Ser. 531, 81–90.
Odate, T., Fukuchi, M., 1995. Distribution and community structure of picophytoplankton in the Southern Ocean during the late austral summer of 1992. Proc. NIPR Symp. Polar Biol. 86–100.
Orsi, A.H., Whitworth Iii, T., Nowlin Jr., W.D., 1995. On the meridional extent and fronts of the Antarctic circumpolar current. Deep-Sea Res. I Oceanogr. Res. Pap. 42, 641–673.
Pardo, P., Tilbrook, B., van Ooijen, E., Passmore, A., Neill, C., Jansen, P., Sutton, A.J., Trull, T.W., 2019. Surface Ocean carbon dioxide variability in South Pacific boundary currents and subantarctic waters. Sci. Rep. 9, 7592.
Patil, S.M., Mohan, R., Shetye, S., Gazi, S., Jafar, S., 2014. Morphological variability of emiliania huxleyi in the indian sector of the Southern Ocean during the austral summer of 2010. Mar. Micropaleontol. 107, 44–58.
Popp, B.N., Kenig, F., Wakeham, S.G., Laws, E.A., Bidigare, R.R., 1998. Does growth rate affect ketone unsaturation and intracellular carbon isotopic variability in emiliania huxleyi? Paleoceanography 13, 35–41.
Pörtner, H., Roberts, D., Masson-Delmotte, V., Zhai, P., Tignor, M., Poloczanska, E., Mintenbeck, K., Nicolai, M., Okem, A., Petzold, J., 2019. Summary for policymakers. IPCC Special Report on the Ocean and Cryosphere in a Changing Climate.
Poulton, A.J., Painter, S.C., Young, J.R., Bates, N.R., Bowler, B., Drapeau, D., Lyczskowski, E., Balch, W.M., 2013. The 2008 emiliania huxleyi bloom along the patagonian shelf: ecology, biogeochemistry, and cellular calcification. Glob. Biogeochem. Cycles 27, 1023–1033.
Prahl, F.G., Wakeham, S.G., 1987. Calibration of unsaturation patterns in long-chain ketone compositions for palaeotemperature assessment. Nature 330, 367–369.
Prahl, F.G., Muehlhausen, L.A., Zahnle, D.L., 1988. Further evaluation of long-chain alkenones as indicators of paleoceanographic conditions. Geochim. Cosmochim. Acta 52, 2303–2310.
Prahl, F.G., Sparrow, M.A., Wolfe, G.V., 2003. Physiological impacts on alkenone paleothermometry. Paleoceanography 18.
Prahl, F.G., Rontani, J.F., Zabeti, N., Walinsky, S.E., Sparrow, M.A., 2010. Systematic pattern in U37K′ – temperature residuals for surface sediments from high latitude and other oceanographic settings. Geochim. Cosmochim. Acta 74, 131–143.
Ridgway, K.R., 2007. Seasonal circulation around Tasmania: an interface between eastern and western boundary dynamics. J. Geophys. Res. Oceans 112.
Rigual Hernández, A.S., Flores, J.A., Sierro, F.J., Fuertes, M.A., Cros, L., Trull, T.W., 2018. Coccolithophore populations and their contribution to carbonate export during an annual cycle in the australian sector of the Antarctic zone. Biogeosciences 15, 1843–1862.
Rigual-Hernández, A.S., Trull, T.W., Bray, S.G., Cortina, A., Armand, L.K., 2015. Latitudinal and temporal distributions of diatom populations in the pelagic waters of the subantarctic and polar frontal zones of the Southern Ocean and their role in the biological pump. Biogeosciences 12, 8615–8690.
Rigual-Hernández, A.S., Trull, T.W., Bray, S.G., Armand, L.K., 2016. The fate of diatom valves in the subantarctic and polar frontal zones of the Southern Ocean: sediment trap versus surface sediment assemblages. Palaeogeogr. Palaeoclimatol. Palaeoecol. 457, 129–143.
Rigual-Hernández, A.S., Sánchez-Santos, J.M., Eriksen, R., Moy, A.D., Sierro, F.J., Flores, J.A., Abrantes, F., Bostock, H., Nodder, S.D., González-Lanchas, A., Trull, T.W., 2020a. Limited variability in the phytoplankton emiliania huxleyi since the pre-industrial era in the subantarctic Southern Ocean. Anthropocene 100254.
Rigual-Hernández, A.S., Trull, T.W., Flores, J.A., Nodder, S.D., Eriksen, R., Davies, D.M., Hallegraeff, G.M., Sierro, F.J., Patil, S.M., Cortina, A., Ballegeer, A.M., Northcote, L.C., Abrantes, F., Rufino, M.M., 2020b. Full annual monitoring of subantarctic emiliania huxleyi populations reveals highly calcified morphotypes in high-CO2 winter conditions. Sci. Rep. 10, 2594.
Rigual-Hernández, A.S., Trull, T.W., Nodder, S.D., Flores, J.A., Bostock, H., Abrantes, F., Eriksen, R.S., Sierro, F.J., Davies, D.M., Ballegeer, A.M., Fuertes, M.A., Northcote, L.C., 2020c. Coccolithophore biodiversity controls carbonate export in the Southern Ocean. Biogeosciences 17, 245–263.
Rintoul, S.R., Trull, T.W., 2001. Seasonal evolution of the mixed layer in the subantarctic zone south of Australia. J. Geophys. Res. Oceans 106, 31447–31462.
Rintoul, S.R., Donguy, J.R., Roemmich, D.H., 1997. Seasonal evolution of upper ocean thermal structure between Tasmania and Antarctica. Deep-Sea Res. I Oceanogr. Res. Pap. 44, 1185–1202.
Roemmich, D., Gilson, J., 2009. The 2004–2008 mean and annual cycle of temperature, salinity, and steric height in the global ocean from the Argo program. Prog. Oceanogr. 82, 81–100.
Rontani, J.-F., Bonin, P., Jameson, I., Volkman, J.K., 2005. Degradation of alkenones and related compounds during oxic and anoxic incubation of the marine haptophyte emiliania huxleyi with bacterial consortia isolated from microbial mats from the camargue, France. Org. Geochem. 36, 603–618.
Rontani, J.-F., Harji, R., Guasco, S., Prahl, F.G., Volkman, J.K., Bhosle, N.B., Bonin, P., 2008. Degradation of alkenones by aerobic heterotrophic bacteria: selective or not? Org. Geochem. 39, 34–51.
Rontani, J.F., Zabeti, N., Wakeham, S.G., 2009. The fate of marine lipids: biotic vs. Abiotic degradation of particulate sterols and alkenones in the northwestern Mediterranean Sea. Mar. Chem. 113, 9–18.
Rontani, J.F., Volkman, J.K., Prahl, F.G., Wakeham, S.G., 2013. Biotic and abiotic degradation of alkenones and implications for U37K′ paleoproxy applications: a review. Org. Geochem. 59, 95–113.
Rosell-Melé, A., Comes, P., Müller, P.J., Ziveri, P., 2000. Alkenone fluxes and anomalous U37K′ values during 1989–1990 in the Northeast Atlantic (48°N 21°W). Mar. Chem. 71, 251–264.
Saavedra-Pellitero, M., Baumann, K.-H., 2015. Comparison of living and surface sediment coccolithophore assemblages in the Pacific sector of the Southern Ocean. Micropaleontology 61, 507–520.
Saavedra-Pellitero, M., Baumann, K.-H., Flores, J.-A., Gersonde, R., 2014. Biogeographic distribution of living coccolithophores in the Pacific sector of the Southern Ocean. Mar. Micropaleontol. 109, 1–20.
Sawada, K., Handa, N., Shiraiwa, Y., Danbara, A., Montani, S., 1996. Long-chain alkenones and alkyl alkenoates in the coastal and pelagic sediments of the northwest North Pacific, with special reference to the reconstruction of emiliania huxleyi and Gephyrocapsa oceanica ratios. Org. Geochem. 24, 751–764.
Schlitzer, R., 2021. Ocean data view. https://odv.awi.de.
Segev, E., Castañeda, I.S., Sikes, E.L., Vlamakis, H., Kolter, R., 2016. Bacterial influence on alkenones in live microalgae. J. Phycol. 52, 125–130.

Siegel, D.A., Deuser, W.G., 1997. Trajectories of sinking particles in the Sargasso Sea: modeling of statistical funnels above deep-ocean sediment traps. Deep-Sea Res. I Oceanogr. Res. Pap. 44, 1519–1541.
Siegel, D.A., Granata, T.C., Michaels, A.F., Dickey, T.D., 1990. Mesoscale eddy diffusion, particle sinking, and the interpretation of sediment trap data. J. Geophys. Res. 95, 5305–5311.
Sikes, E.L., Volkman, J.K., 1993. Calibration of alkenone unsaturation ratios (Uk'37) for paleotemperature estimation in cold polar waters. Geochim. Cosmochim. Acta 57, 1883–1889.
Sikes, E.L., Volkman, J.K., Robertson, L.G., Pichon, J.-J., 1997. Alkenones and alkenes in surface waters and sediments of the Southern Ocean: implications for paleotemperature estimation in polar regions. Geochim. Cosmochim. Acta 61, 1495–1505.
Sikes, E.L., Howard, W.R., Neil, H.L., Volkman, J.K., 2002. Glacial-Interglacial Sea surface temperature changes across the subtropical front east of New Zealand based on alkenone unsaturation ratios and foraminiferal assemblages. Paleoceanography 17, 2-1-2-13.
Sikes, E.L., O'Leary, T., Nodder, S.D., Volkman, J.K., 2005. Alkenone temperature records and biomarker flux at the subtropical front on the Chatham rise, SW Pacific Ocean. Deep-Sea Res. I Oceanogr. Res. Pap. 52, 721–748.
Sikes, E., Howard, W., Samson, C., Mahan, T., Robertson, L., Volkman, J., 2009. Southern Ocean seasonal temperature and Subtropical Front movement on the South Tasman Rise in the late Quaternary. Paleoceanogr. Paleoclimatol. 24.
Sikes, E.L., Schiraldi Jr., B., Williams, A., 2019. Seasonal and latitudinal response of New Zealand Sea surface temperature to warming climate since the last glaciation: comparing alkenones to Mg/Ca foraminiferal reconstructions. Paleoceanogr. Paleoclimatol. 34, 1816–1832.
Sonzogni, C., Bard, E., Rostek, F., Dollfus, D., Rosell-Melé, A., Eglinton, G., 1997. Temperature and salinity effects on alkenone ratios measured in surface sediments from the Indian Ocean. Quat. Res. 47, 344–355.
Sukenik, A., Wahnon, R., 1991. Biochemical quality of marine unicellular algae with special emphasis on lipid composition. I. Isochrysis galbana. Aquaculture 97, 61–72.
Tamsitt, V., Talley, L.D., Mazloff, M.R., 2019. A deep eastern boundary current carrying indian deep water south of Australia. J. Geophys. Res. Oceans 124, 2218–2238.
Tierney, J.E., Tingley, M.P., 2018. BAYSPLINE: a new calibration for the alkenone paleothermometer. Paleoceanogr. Paleoclimatol. 33, 281–301.
Trull, T.W., Bray, S.G., Manganini, S.J., Honjo, S., François, R., 2001a. Moored sediment trap measurements of carbon export in the subantarctic and polar frontal zones of the Southern Ocean, south of Australia. J. Geophys. Res. Oceans 106, 31489–31509.
Trull, T.W., Rintoul, S.R., Hadfield, M., Abraham, E.R., 2001b. Circulation and seasonal evolution of polar waters south of Australia: implications for iron fertilization of the Southern Ocean. Deep-Sea Res. II Top. Stud. Oceanogr. 48, 2439–2466.
Trull, T.W., Bray, S.G., Buesseler, K.O., Lamborg, C.H., Manganini, S., Moy, C., Valdes, J., 2008. In situ measurement of mesopelagic particle sinking rates and the control of carbon transfer to the ocean interior during the vertical flux in the Global Ocean (VERTIGO) voyages in the North Pacific. Deep-Sea Res. II Top. Stud. Oceanogr. 55, 1684–1695.
Trull, T.W., Schulz, E., Bray, S.G., Pender, L., McLaughlan, D., Tilbrook, B., Rosenberg, M., Lynch, T., 2010. The Australian Integrated Marine Observing System Southern Ocean Time Series facility, OCEANS 2010 IEEE - Sydney, pp. 1–7.
Turner, J.T., 2002. Zooplankton fecal pellets, marine snow and sinking phytoplankton blooms. Aquat. Microb. Ecol. 27, 57–102.
Turner, J.T., 2015. Zooplankton fecal pellets, marine snow, phytodetritus and the ocean's biological pump. Prog. Oceanogr. 130, 205–248.
van Sebille, E., England, M.H., Zika, J.D., Sloyan, B.M., 2012. Tasman leakage in a fine-resolution ocean model. Geophys. Res. Lett. 39.
Versteegh, G.J.M., Riegman, R., de Leeuw, J.W., Jansen, J.H.F., 2001. U37k′ values for Isochrysis galbana as a function of culture temperature, light intensity and nutrient concentrations. Org. Geochem. 32, 785–794.
Volkman, J.K., Eglinton, G., Corner, E.D.S., Forsberg, T.E.V., 1980. Long-chain alkenes and alkenones in the marine coccolithophorid emiliania huxleyi. Phytochemistry 19, 2619–2622.
Volkman, J.K., Barrerr, S.M., Blackburn, S.I., Sikes, E.L., 1995. Alkenones in Gephyrocapsa oceanica: implications for studies of paleoclimate. Geochim. Cosmochim. Acta 59, 513–520.
Wang, K.J., Huang, Y., Majaneva, M., Belt, S.T., Liao, S., Novak, J., Kartzinel, T.R., Herbert, T.D., Richter, N., Cabedo-Sanz, P., 2021. Group 2i isochrysidales produce characteristic alkenones reflecting sea ice distribution. Nat. Commun. 12, 15.
Wynn-Edwards, C.A., Shadwick, E.H., Davies, D.M., Bray, S.G., Jansen, P., Trinh, R., Trull, T.W., 2020. Particle fluxes at the australian Southern Ocean time series (SOTS) achieve organic carbon sequestration at rates close to the global median, are dominated by biogenic carbonates, and show no temporal trends over 20-years. Front. Earth Sci. 8, 329.
Young, J., Geisen, M., Cross, L., Kleijne, A., Sprengel, C., Probert, I., Østergaard, J., 2003. A Guide to Extant Coccolithophore Taxonomy. International Nannoplankton Association.
Young, J.R., Bown, P.R., Lees, J.A., 2021. In: Association, I.N. (Ed.), Nannotax3 Website.
Yu, E.F., Francois, R., Bacon, M.P., Honjo, S., Fleer, A.P., Manganini, S.J., Rutgers van der Loeff, M.M., Ittekot, V., 2001. Trapping efficiency of bottom-tethered sediment traps estimated from the intercepted fluxes of 230Th and 231Pa. Deep-Sea Res. I Oceanogr. Res. Pap. 48, 865–889.
Ziveri, P., de Bernardi, B., Baumann, K.-H., Stoll, H.M., Mortyn, P.G., 2007. Sinking of coccolith carbonate and potential contribution to organic carbon ballasting in the deep ocean. Deep-Sea Res. II Top. Stud. Oceanogr. 54, 659–675.